Phase Planes in the universe: Chaotic Cyclic universes and Kicking Chameleons

Emma Platts

Supervised by Prof. Amanda Weltman and Prof. George F.R. Ellis

2015

Abstract

This thesis consists of two main sections: chaotic cyclic cosmology and Chameleon gravity in the early universe. Both sections invoke a phase plane analysis as their commonality. The first explores a cyclic model, proposed by Ellis et al. [1], that is in keeping with current observations. No exotic nor new physics is needed for the bounce nor the turnaround. The model is chaotic in nature and requires only that the universe is closed and that dark energy (at some time) decays. The second section contests the claim by Burrage et al. [2,3] that Chameleon gravity is inconsistent in the early universe, unless constraints on its coupling mechanism are significantly increased. It is shown that the addition of a Dirac-Borne-Infeld (DBI) correction — a consistent, high energy modification — to the Chameleon dynamically renders it weakly coupled to matter [4]. This is done without any fine-tuning and ensures the consistency of the Chameleon at all scales without infringing upon its crucial feature as a dark energy candidate: its elusive but prominent coupling to matter.

Contents

1 Introduction

Phase planes are a powerful tool in the numerical analysis of nonlinear systems and their characteristics, which cannot be solved analytically. The portraits are user-friendly, providing a visual display of solutions to differential equations and hence are useful in determining the behaviour of physical systems. Since they are applicable to these nonlinear and physical systems, phase planes prove to be invaluable in a vast array of fields, with the focus of this thesis exploring arguably one of the most profound: cosmology.

1.1 Cosmology

Cosmology, a serious field of study for only the last century, has rapidly evolved to become a precision science that unabashedly confronts the biggest questions of life. Seeking to understand the origins, evolution and large scale structure of the universe, modern cosmology has made tremendous progress since its beginnings with Albert Einstein in 1917 [5].

Einstein's theory of general relativity prompted physicists to re-examine theories of the origins of the universe while advancing technology allowed astronomers to observe very distant objects. With the initial theory of an expanding universe introduced by Friedmann in 1922 [6], the age-old belief of a static universe was finally dislodged by the confrontation with Hubble's discovery of redshift in 1929 [7]. This corroborated Lemaître's Big Bang theory, proposed in 1927 [8], which to date remains the prevailing scientific model for the early development of the universe.

In the 1990s, dramatic advances in observational cosmology allowed for precise agreement between theory and observation, firmly shaping cosmology into a predictive science. This has become known as the golden age of cosmology; where cosmology before consisted of speculations, it is now a hard science, with theories developed and tested against precise data. These revolutionary advances include

- observations of the cosmic microwave background (CMB) with COBE [9], WMAP [10] and Planck [11],
- large new galaxy redshift surveys such as 2dfGRS [12] and SDSS [13],
- observations of distant supernovae [14] and gravitational lensing [15].

In revolutionising cosmology with the discoveries and solutions unveiled by these observations, a whole new plethora of mysteries was revealed, too.

1.2 Problems, solutions and mysteries

1.2.1 The horizon problem

The horizon problem, identified in the late 1960s by Charles Misner [16], points out that different regions of the sky have not been in contact due to the large distances between them, and yet they each display the same temperature and physical properties. With information propagation limited by the speed of light, this causal connection should not be possible.

To illustrate this more clearly, consider looking into the night sky. The distances observed correspond to time in the past due to light taking time to reach us. Observing two galaxies both at 10 billion light years away and in opposite directions, one finds that the time for light (or information)

to travel from one galaxy to the other is 20 billion years. This is, however, longer than the age of the universe.

The theory of inflation resolves this issue, with CMB observations confirming its likelihood. The CMB is an emission of uniform, black body thermal energy from all parts of the sky, left over from the time of recombination in the early universe. It is observed to be isotropic to 1 part per 100 000, with only very small fluctuations. This means that the very early universe was remarkably homogeneous before undergoing a period of exponential expansion. The universe was small and in causal connection, with inflation rapidly increasing its size, while conserving its uniformity at large distances.

1.2.2 The flatness problem

This fine-tuning problem, first brought up by Robert Dicke in 1969, notes that a very specific critical value of the matter and energy density is required in order for the universe to be flat. As the universe evolves with cosmic time, the density moves quickly away from the required critical density. In fact, the required initial density would have to vary from the critical value by one part in 10^{62} or less in order to obtain today's conditions. That one observes a flat universe despite this unfathomably small likelihood is commonly explained with inflation, where the density is driven close enough to the required critical value. There are, however, many gaps in inflationary theory that still need to be filled. Cosmologists have yet to establish any firm evidence of the inflaton — the field that drives inflation — and many of the proposed versions of the theory themselves contain parameters or initial conditions that require a fine-tuning.

1.2.3 The problem of missing mass

One of the greatest cosmological conundrums is that the apparent mass of the universe is significantly different from the observed mass. In 1933, Fritz Zwicky applied the virial theorem to the Coma cluster [17] [1]. He estimated its mass based on the motions of the galaxies and compared this to apparent mass obtained from the brightness and number of galaxies. He found a large discrepancy, giving the first formal inference of the missing mass problem, with a significant portion of the universe's matter 'dark'.

In the 1960s and 1970s, Rubin and Ford used galaxy rotation curves to confirm robustly Zwicky's findings [18, 19]. As stars get further from the center of the galaxy, it was found that their velocities do not decrease according to the usual inverse square rule, but instead remain approximately constant. This observation suggests either that there is mass in the universe that we cannot detect or that the standard theory of gravity is lacking.

There have been various proposals to solve this problem of missing mass in the form of dark matter theories and modified gravity theories. The most popular of the latter, modified Newtonian dynamics (MOND) [20], does not account for observed properties of galaxy clusters and there is yet to be a satisfactory cosmological model constructed from the theory. Dark matter, contributing 26.8% to the total energy of the universe, is more universally accepted to be the solution to the missing mass problem. The strongest candidates for dark matter include weakly interacting massive particles (WIMPs) [21, 22] and axions [23, 24], however evidence for either is yet to be found.

[1] Cited is the widely read second version. The original, in German, appeared in an obscure journal named *Helvetica physica acta, vol. 6, p. 110.*

1.2.4 The accelerated expansion of the universe

The age-old belief in a static universe has been dislodged by a confrontation with data that reveals the universe is not only dynamic and evolving, but is presently accelerating in its expansion. This was confirmed by the 1998 observation of Type 1a supernovae [14, 25–27], complimented by independent evidence from the CMB, gravitational lensing and large galaxy redshift surveys. The expansion is driven by an unobserved energy that accounts for an astounding 68.3% of the energy of the universe. Dark energy is explained by invoking the use of Einstein's once disregarded cosmological constant, or introduces quintessence or modified gravity theories.

The cosmological constant is the value of the vacuum energy density of space, with a negative pressure that causes the expansion of the universe to accelerate. Although this is currently the standard model of cosmology, known as ΛCMD cosmology, it does have a major outstanding problem. Namely, physicists commonly assume that the quantum vacuum is equivalent to the cosmological constant, however quantum theories predict a value that is 100 orders of magnitude too big. Further, supersymmetric theories require a cosmological constant that is exactly zero. That there is no natural emergence of this tiny constant from fundamental physics is worrying, and has given rise to alternative dark energy models.

Quintessence models have a dynamical field whose potential energy causes the observed acceleration of the universe [28,29]. This quintessence has been proposed as a fifth fundamental force and in contrast to the cosmological constant, changes over time. Also proposed are a wealth of modified theories of gravity, such as $f(R)$ gravity, scalar-tensor theories, braneworld gravity, Galileon gravity and more. Despite the resources and vast number of skilled researchers dedicated to finding the mysterious force behind our universe's accelerated expansion, the puzzle remains unsolved.

1.2.5 The curvature of the universe

Though the universe is found to be remarkably close to flat, it is infinitesimally likely that it is exactly flat, and despite our best efforts, the question of whether our universe is spatially open or closed is yet to be resolved. This distinction holds crucial information about the future of our universe and could be used to rule out a wide range of cosmological models. That there is not a greater focus in determining the curvature of the universe is itself a mystery, and this will be discussed in Section 2.

1.3 Going forward

Although we have come a long way in the past century, it is clear there is still much ground to be covered. One should not, however, be discouraged. With questions come eventual answers, and the pursuit thereof brings us ever closer to understanding our universe and mankind's place within it. For the ambitious, this also means that there are many Nobel Prizes waiting to be won.

In the sections to follow, it will be shown that phase plane analysis can serve to bring us closer to solving these mysteries. Two areas of cosmology are considered: cyclic universes (Section 2) and Chameleon gravity (Section 3). Both problems, though vastly different in nature, utilise phase planes throughout in order to draw their conclusions. The cyclic cosmology explored is chaotic and is in keeping with current observations. It emerges naturally in an open universe with a decaying cosmological constant, and does not invoke any exotic physics for the bounce or turnaround [1]. This picks up on two of the aforementioned problems: that the curvature of the universe it yet to

be deduced and that the fate of the universe is still unknown. The viability of such a model is important as it brings us closer to understanding the nature of our universe. Could the universe be cyclic, or does it simply expand indefinitely?

Section 3 deals with Chameleon gravity (a scalar-tensor theory), and serves to preserve the Chameleon's viability as a dark energy model. Recently, doubts were raised regarding the Chameleon's consistency prior to Big Bang Nucleosynthesis (BBN) [2, 3], however it is shown that the addition of a UV-correction ensures that the Chameleon remains a robust theory without having to place restrictive constraints on its mechanism [4].

It is important to note that these sections are entirely disjoint, with the analysis tool and the broader topic of cosmology being their only commonalities. A standard ΛCDM cosmology is used in Section 2 and modified gravity in Section 3. Section 2 could be recast using a theory of modified gravity, but one of its main intriguing features is that it is consistent with standard theory.

2 Chaotic Cyclic Cosmology

2.1 Introduction

2.1.1 Overview

Despite the plethora of available data, questions about the origin of our universe remain unresolved. Further more, we do not yet understand the nature of our universe, and so questions regarding its fate are open, too. The possible scenarios are;

1. the universe will expand indefinitely, approaching heat death;
2. it will collapse into a singularity; or
3. it will have cycles in which it expands, collapses, bounces and re-expands.

Dark energy suggests that the first is most likely, however observations have yet to rule out the last; cyclic universes.

On the largest scales, the universe respects the cosmological principle, with an appearance that is homogeneous and isotropic. Observations show that the universe is dynamic, having evolved through different characteristic phases, each dominated by a particular matter type. We also appear to live in a universe that is remarkably close to flat. As previously mentioned, the best explanation for this is given by a phase of inflation; the rapid expansion of the very early universe that lasted at least 60 efolds[2] [30–33]. Succeeding this were a radiation-, a matter- and, presently, a dark energy dominated era. Although a singularity is typically assumed prior to inflation, a variety of cyclic universes [34–38] have yet to be ruled out. All of these, however, invoke new physics in order to produce a satisfactory bounce mechanism as well as a model of transition from the current phase of accelerated expansion to a collapsing phase.

Working together with A. Weltman, G.F.R. Ellis and D. Sloan, we developed a cyclic universe model that is reasonable from a dynamical systems perspective [1]. This model relies on standard cosmological assumptions, with only two conditions:

1. The spatial sections must have positive curvature ($\Omega_k = +1$).

[2] An efold is the time interval in which the expanding universe has grown by a factor of e.

2. The late time effective cosmological constant must decay fast enough as a function of the scale factor.

Both of these conditions are consistent with current measurements, as can be confirmed with the following data.
For the curvature with a constant equation of state $w(a) = w_0$, one has [39]

$$\Omega_k = 0.006^{+0.012+0.032}_{-0.013-0.025} \tag{2.1}$$

and for $w(a) = w_0 + w_a(1-a)$, one has [39]

$$\Omega_k = 0.002^{+0.018+0.032}_{-0.018-0.041}. \tag{2.2}$$

For the equation of state [11, 40]

$$w := \frac{p}{\rho} = -1.006^{+0.085}_{-0.091}\,,\ \frac{dw}{da} = 0.03^{+0.68}_{-0.40}. \tag{2.3}$$

One should note that these constraints are, however, very model-dependent.

2.1.2 Chronology of the universe

Initially, in accordance with the prevailing standard scientific theory, the chronology of the universe shall be assumed to be a big bang, followed by inflation [7,8,30–33]. After the singularity and before inflation, little is known about the universe. The universe was so hot (at temperatures of $\sim 10^{15}$K) that no particles could exist with any sort of stability, and the four fundamental forces are believed to have existed as a single "unified force". It may be that a period of radiation preceded inflation. Though this is not required for successful inflation, this possibility will be included to consider the effects on the dynamics. During cosmological inflation the universe increased in size by a factor of at least 10^{27} [30–33]. After inflation, the universe returned to radiation dominance until it cooled to a point that allowed the forces to undergo symmetry breaking, eventually causing the separation of the strong force from the electroweak force. This meant that the first stable particles could finally exist in a quark-gluon plasma. The universe continued to cool until the four forces took their present forms, and the spectacular range of particles we know today could become possible. This led to the universe, at last, being matter dominated, with the densities of non-relativistic matter and radiation equal. Recombination then took place, with the emergence of the first neutral atoms. By the end of recombination, most of the protons were bound in these neutral atoms, allowing for previously scattered photons to escape freely into space, making the universe transparent. This is known as decoupling, with these photons still detectable today in the cosmic microwave background. This CMB was detected in 1965 by Penzias and Wilson — a landmark test of the Big Bang model [41]. With the fundamental particles and forces in place, the universe continued to expand, giving rise through cosmic evolution to the first stable large-scale structures, such as stars, quasars and galaxies. As for the future of our universe, there are several different theories.

Stars will eventually die, and fewer will be born to replace them. This will lead to a darkening universe, and the eventual end of the Stelliferous Era. After this, there are a number of possible outcomes. Initially, before the discovery of the accelerating expansion of the universe, there were two main competing models to describe the fate of the universe; the "big crunch" and the "big freeze" (or heat death). The big crunch assumes that the overall density of the universe is large enough such that it will eventually cease to expand and instead begin to contract. This symmetric theory then sees the collapse of space-time into a singularity. Heat death, on the other hand, holds the view that the universe will continue to expand and gradually approach absolute zero temperature. Eventually, in a state of maximum entropy, the universe will no longer be able to sustain

life, leaving the universe to disintegrate into empty space and weak radiation, infinitesimally close to absolute zero temperature.

In order to decide the most likely model, astronomers in the early 1990's calculated the total mass density of the universe. The low density detected lead them to believe that heat death is the most likely scenario. It was not long after however, with the initial discovery in 1998, that the universe was found to be expanding at an accelerating rate [42–44]. The observations of the Type Ia supernovae confirm this, with the widely accepted belief that dark energy is accountable [27]. With dark energy, heat death is confirmed as being the likely fate of our universe, with the universe expanding at an ever increasing rate and all matter and radiation fading away.

However, all is not lost! There exists an alternative to the ever-expanding universe theory; a cyclic universe, which undergoes successive cycles of expansion and collapse. Such models have been widely explored in the past century (see for example [34–37, 45–54]). In many ways these models are more satisfactory. The current theory that our universe, in its spectacular beauty and mystery, dies not with a bang but with a whimper, leaves one wanting. Further, a universe that perhaps has always been and always will be is arguably more intuitive than one that explodes out of nothingness and continues to expand indefinitely into the unknown.

2.1.3 Modelling the chronology of the universe

The chronology described above can be divided into five epochs, each defined by its dominant matter type; radiation, inflation, radiation, matter and dark energy. This is modelled following the phase plane technique of Madsen and Ellis [55], with the addition of a cosmological constant Λ dominated phase. The case for which the cosmological constant is decaying is also explored. Current literature no longer includes a radiation dominated era prior to inflation, however, in keeping with Madsen and Ellis [55], this phase will initially be included it allows for a simple representation of emergent universe models [56–58].

2.2 Phase plane equations

Assuming an FLRW universe described by a scale factor a, Hubble parameter $H \equiv \dot{a}/a$, and the energy-momentum tensor for a perfect fluid, T^{μ}_{ν} =diag$(\rho, -p, -p, -p)$, the Friedmann, Raychaudhuri, and conservation equations are, respectively,

$$H^2 = \frac{8\pi G\rho}{3} - K, \tag{2.4}$$

$$3\dot{H} + 3H^2 + \frac{8\pi G}{2}\Big(\rho + 3p\Big) = 0, \tag{2.5}$$

$$\dot{\rho} + 3H(\rho + p) = 0. \tag{2.6}$$

Here ρ is the total energy density and p is the total pressure. The curvature, $K = k/a^2$, is set by the value of the constant k, i.e. $k > 0$ for a closed universe, $k = 0$ for a flat universe and $k < 0$ for an open universe. The derivation of these equations from Einstein's field equations are in A.1.

Defining the equation of state $w \equiv -p/\rho$, one should note that it varies with epoch. Since the scale factor $a(t)$ determines conditions at a time t, the equation of state is written $w = w(a)$. Initially, each epoch will be treated as having a constant equation of state as determined by the dominant matter type. With $\kappa \equiv 8\pi G$, the total density parameter Ω is defined as

$$\Omega \equiv \frac{\kappa\rho}{3H^2}. \tag{2.7}$$

Inserting this into equation 2.4, one arrives at

$$K = H^2(\Omega - 1). \tag{2.8}$$

This can be written in terms of the spatial curvature density $\Omega_K = \frac{K}{H^2}$ as

$$\Omega_K = \Omega - 1. \tag{2.9}$$

By examining the above equation one can see that $\Omega_K < 0$ if $\Omega < 1$, $\Omega_K = 0$ if $\Omega = 1$ and $\Omega_K > 0$ if $\Omega > 1$; the cases for negative, flat, and positive spatial curvature respectively. If the spatial sections have their simply connected natural topology, these are also the cases of open, flat, and closed universes respectively.

Using the conservation equation (B.15) and Raychaudhuri equation (2.5), one finds the derivative of the density parameter Ω to be given by

$$\dot{\Omega} = -H\Omega(1 - \Omega)(1 + 3w). \tag{2.10}$$

This, together with $\dot{a} = Ha$ from the definition of Hubble's parameter, forms the system of differential equations for the phase planes.

Note that for any equation of state $\Omega = 0$ (an empty model) and $\Omega = 1$ (flat spatial sections) are solutions with constant Ω. Also $w = -1/3$ and $H = 0$ imply that Ω is constant, whatever its value.

2.3 Phase planes for epochs with a constant equation of state

In order to create the phase planes, it is assumed that the equation of state is constant in each epoch, each of which is defined by initial and final values of the Robertson-Walker scale factor. The epochs each correspond to when the universe was dominated by a particular simple, one-component field, as previously discussed.

2.3.1 Standard matter case: $w > -1/3$

Standard matter has $w \geq 0$, but the phase diagram stays the same provided $w > -1/3$. Important examples are $w = 0$ and $w = 1/3$ for pressure-free matter (dust) and pure radiation, respectively. In Figure 1a one can see that $\Omega = 1$ is always an unstable asymptote; the curves cannot cross this line. For $\Omega > 1$ the curves increase monotonically, diverging to infinity for finite values of a (where a maximum occurs as $H \to 0$). For $\Omega < 1$, the curves decrease monotonically towards $\Omega = 0$ as $a \to \infty$.

2.3.2 Inflationary case: $-1 \leq w < -1/3$

Inflation requires a phase of accelerated expansion with an equation of state with negative pressure such that $w < -1/3$ and physical plausibility requires $w \geq -1$. In order to agree with observations of the spectral index, one requires an equation of state $w \approx -1$ [59]. In Figure 1b, all curves monotonically tend to the stable asymptote $\Omega = 1$, so they tend to spatial flatness. They cannot cross this line, as illustrated in 1b, hence should the universe have been open prior to inflation ($k = -1 \Leftrightarrow \Omega < 1$, see equation 2.8), the universe will always remain open.

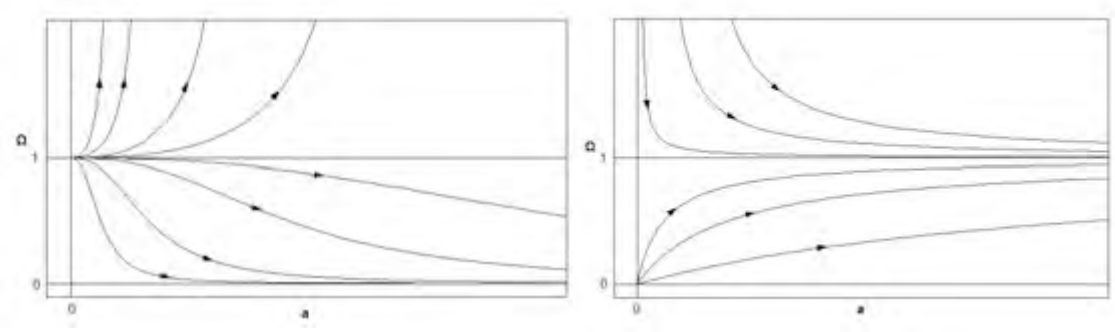

(a) $w = 0$ (b) $w = -1$

Figure 1: Phase planes for dust $w = 0$ and slow roll inflation $w = -1$, respectively

2.4 A Cosmological Constant

Next the current late time phase of accelerated expansion of the universe is examined. This is usually attributed to dark energy [42–44].

2.4.1 The phase plane equations with dark energy

Dark energy theories include a simple cosmological constant or some evolving field; see for example [29, 60–64]. With a cosmological constant Λ, the Friedmann, Raychaudhuri and conservation equations (2.4, 2.5, and B.15) become

$$H^2 = \frac{\kappa\rho}{3} - K + \frac{\Lambda}{3}, \tag{2.11}$$

$$\dot{H} + H^2 + \frac{\kappa}{6}\Big(\rho + 3p\Big) - \frac{\Lambda}{3} = 0, \tag{2.12}$$

$$\dot{\rho} = -3H\rho(1+w) - \frac{\dot{\Lambda}}{\kappa}. \tag{2.13}$$

One can represent a cosmological constant either as a fluid with density ρ and pressure $p = -\rho$, or by the term Λ. Following the latter course and defining

$$\Omega_\Lambda = \frac{\Lambda}{3H^2} \tag{2.14}$$

one finds the modified total density parameter 2.7;

$$\Omega = \frac{\kappa\rho}{3H^2} + \frac{\Lambda}{3H^2}. \tag{2.15}$$

Inserting this into 2.11, one again obtains

$$K = H^2(\Omega - 1) \tag{2.16}$$

and hence

$$\Omega_K = \Omega - 1. \tag{2.17}$$

The modified equation 2.10 for $\dot{\Omega}$ is therefore

$$\dot{\Omega} = -H\left(\Omega - \Omega_\Lambda\right)(1-\Omega)\left(1 + 3w - \frac{2\Omega_\Lambda}{\Omega - \Omega_\Lambda}\right) \tag{2.18}$$

For the rest of this section the case of a cosmological constant ($\dot{\Lambda} = 0$) is considered and in the next section, the case of dynamical dark energy ($\dot{\Lambda} \neq 0$) is considered.

2.4.2 A pure cosmological constant: $\Omega = \Omega_\Lambda$

First considered is the simplest case, where the acceleration is driven by the cosmological constant, Λ. For a pure cosmological constant dominated epoch, $\rho = 0$ and $\dot{\Lambda} = 0$ in the above equations. This yields Figure 2*a*. For all values of Ω the universe expands, with the ultimate fate corresponding to a de Sitter exponentially expanding end state. The spatial curvature is positive for $\Omega > 1$ and negative for $\Omega < 1$.

2.4.3 Matter plus a cosmological constant: $\Omega = \Omega_m + \Omega_\Lambda$

Given current observations, it is perhaps more pertinent to consider a universe made up of both matter and dark energy. Solving 2.18 for the case of a cosmological constant ($\dot{\Lambda} = 0$) and pressure-free matter ($w = 0$), the results are presented in Figure 2b, with matter causing the density to initially increase for $\Omega > 1$, but the curve $\Omega = 1$ is still the final asymptote.

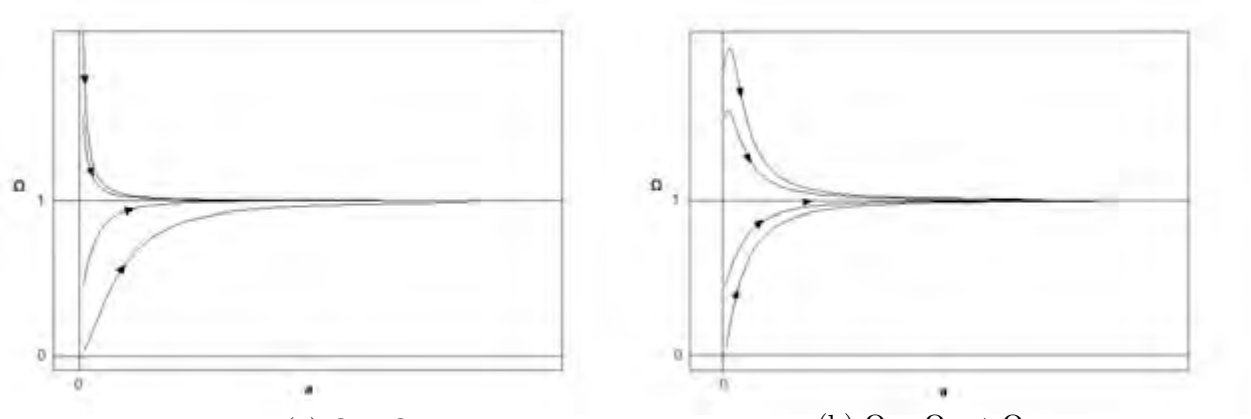

(a) $\Omega = \Omega_\Lambda$ (b) $\Omega = \Omega_m + \Omega_\Lambda$

Figure 2: Phase planes for pure cosmological constant, and for matter and a cosmological constant, respectively.

2.5 All the phases

Putting together the phase portraits for each epoch, a phase plane is created for the entire history of the universe and the current late time with a cosmological constant. This then predicts the future of our universe.

2.5.1 A true cosmological constant

Five phases are represented, each with suitable matter choices, namely;

1. A radiation dominated phase before inflation starts;
2. The inflationary epoch;
3. A radiation dominated Hot Big Bang epoch;
4. A matter dominated epoch;
5. A late time cosmological constant dominated epoch.

They are joined together by suitable junction conditions to give the whole diagram in Figure 3, which updates the image as found in Madsen and Ellis [55] to include a cosmological constant. Note that the scale for a is non-linear, and hence the apparent duration of each epoch is not to scale.

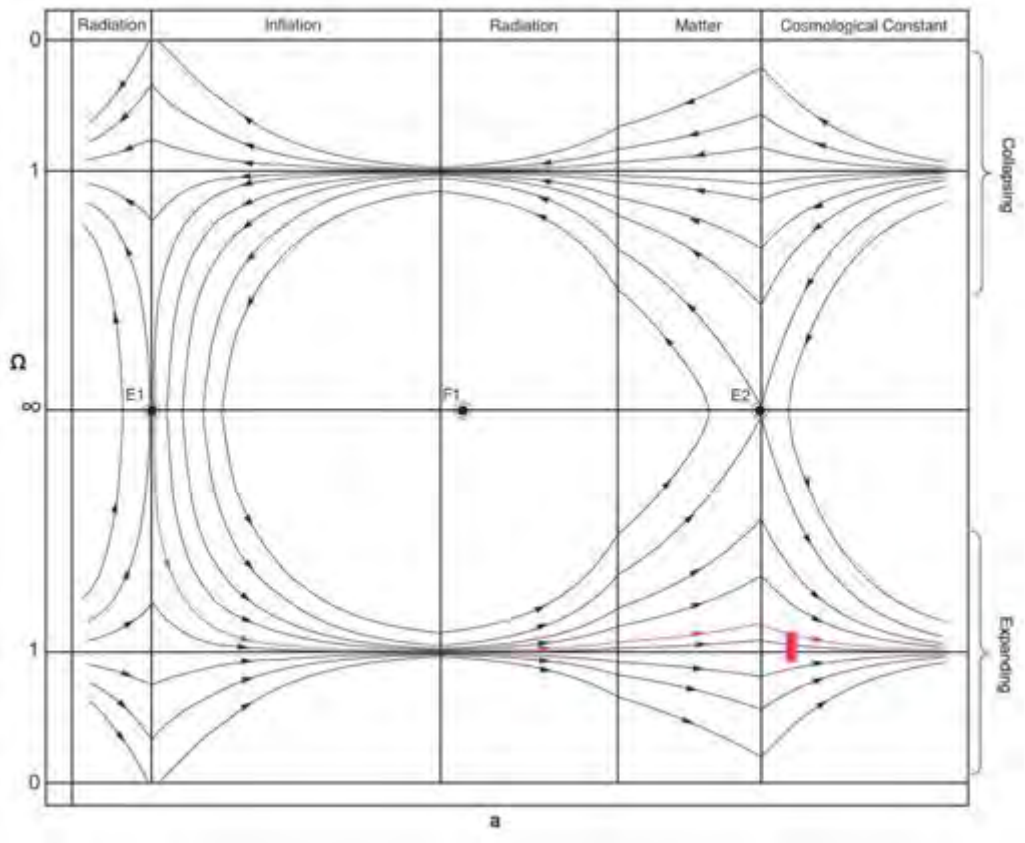

Figure 3: Time symmetric phase plane with a true cosmological constant

A time-symmetry between the collapsing and expanding phases is assumed, as in Madsen and Ellis [55]. It is thus of interest to transform the infinities of Ω (created because $H = 0$ at a point of maximum expansion, explained below) to finite values, using the variable change $\omega = \arctan(\log(\Omega))$. This creates a time-symmetric phase plane for states of expansion and collapse, joined at the boundary $\Omega = \infty$ as shown in Figure 3. The top half of the diagram shows collapsing universes, and the bottom half, expanding universes. There are two saddle points (Einstein static universes $E1$ and $E2$) and a centre $F1$. The direction of flow means that, except for the separatrix that ends up at $E2$, for $\Omega > 1$, a universe in the matter dominated epoch makes a transition from an expanding universe to a contracting one if it reaches $\Omega = \infty$. This occurs when the Hubble parameter is zero ($\dot{a} = 0$) and so the density parameter Ω is infinite (this is therefore just a coordinate singularity because of the representation (2.7)). If it does not reach $\Omega = \infty$, it expands forever with Ω asymptoting to unity, as do all models with $\Omega < 1$. The line $\Omega = 1$ is an attractor during the cosmological constant dominated epoch, as it was during inflation.

The source on the left-hand side is an initial radiative Einstein-de Sitter universe, and the sink on the right-hand side is a final de Sitter universe. This diagram shows the symmetry of some closed matter dominated universes that cycle (expand, reach a maximum, and then collapse), however these do not correspond to the observable universe, plainly because their observed history does

not correspond with our own. There are three fixed points: two Einstein static universes $E1$ and $E2$, which are solutions of the field equations, and the centre $F1$, which is not. The fixed point $F1$ is due to the change of equation of state between matter dominated and a cosmological constant, and has closed cycles around it. The red solution beginning at the Einstein static universe $E1$ corresponds to the emergent universe scenario [56–58], where the universe starts off asymptotically as an Einstein static universe, passes through a phase like that we observe today, and ultimately tends towards a flat universe, expanding forever due to the ultimate dominance of the cosmological constant. These can correspond to the universe today.

One should note that there are models that exist for any measured Ω_{Total} at the present day. The red bar represents our current point in the evolution of the universe, according to present observations. It includes an emergent universe but no cyclic models. Those cyclic models that occur do not have a late time cosmological constant dominated era.

2.5.2 Phase planes with a decaying cosmological constant

So far a relatively standard picture has been explored. Now a dynamical dark energy in the form of a decaying cosmological constant is considered. Again $\Omega = \Omega_m + \Omega_\Lambda$ is used to represent matter plus an effective cosmological constant. The dynamic cosmological constant decays away as

$$\Lambda(a) = \Lambda_0 e^{-Ba}, \tag{2.19}$$

where a is the scale factor and B is a constant.

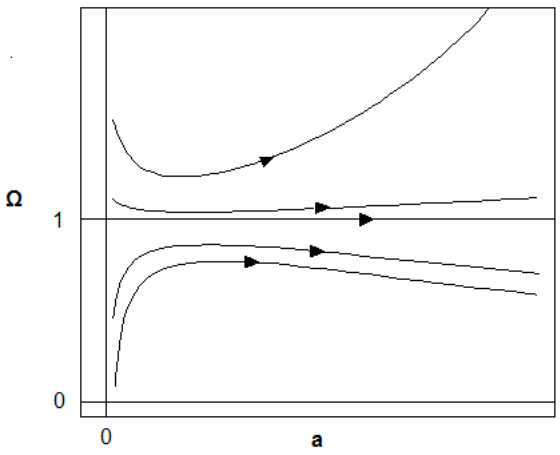

Figure 4: Phase plane for $\Omega = \Omega_m + \Omega_\Lambda$ with Λ decaying

The equation of state for the system is given by

$$w = \frac{Ba}{3} - 1. \tag{2.20}$$

For sufficiently small choices of B the equation of state is $w = -1$ to start and evolves to $w = 0$ as Λ decays. Matter begins to dominate at $a = 3/B$. Beyond $a = 6/B$ the effective equation of state would have $w > 1$, and such a model would be invalid. The phase diagram is shown in Figure 4. The curves diverge away from $\Omega = 1$.

2.5.3 Time symmetric universe with decaying cosmological constant

The method used in Section (2.5) is repeated, but with a decaying Λ of the form (2.19) at late times. Again a time symmetric portrait is created (Figure 5). Here it is assumed that the universe is inflationary from the start, and so this time a pre-inflation radiation dominated epoch is excluded. The results become quite interesting.

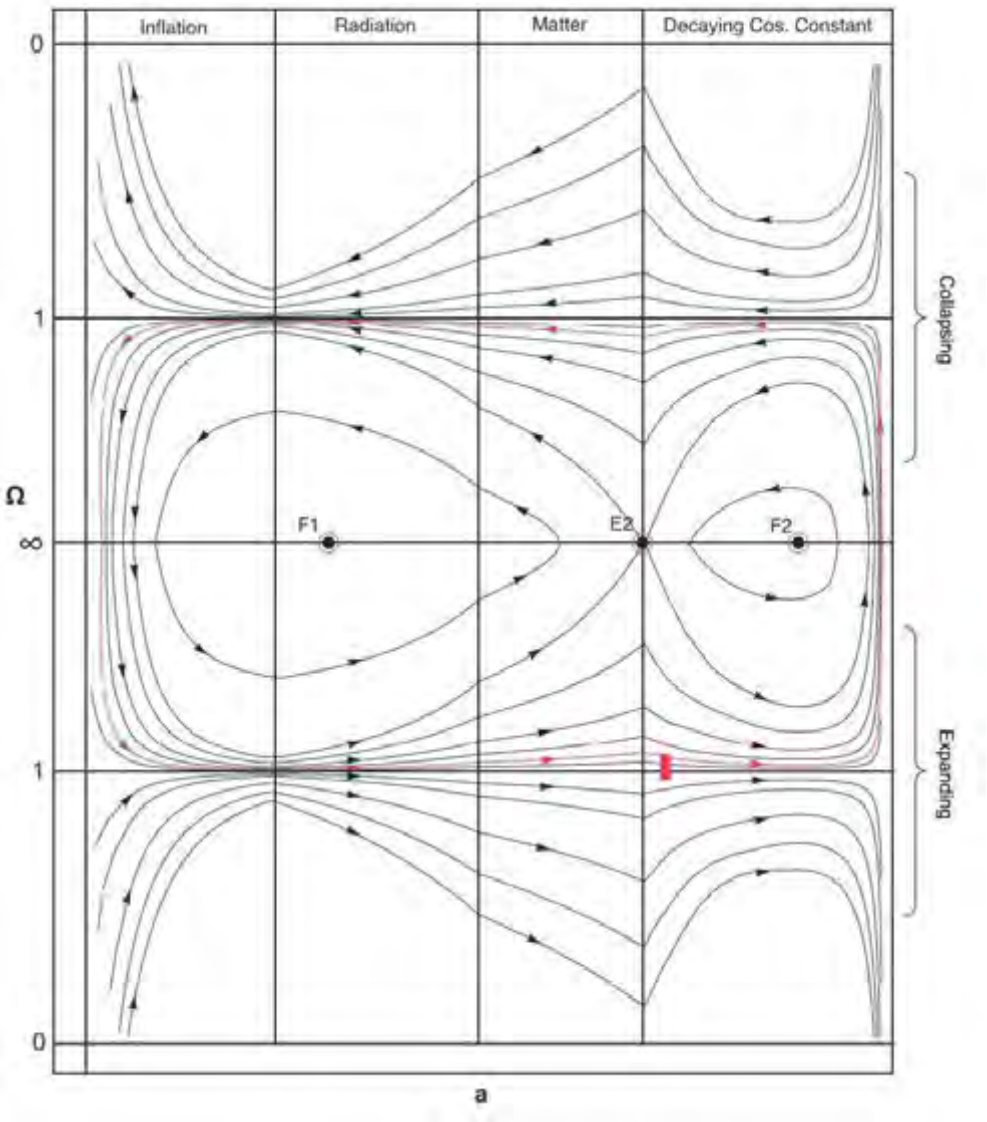

Figure 5: Time symmetric phase plane with a decaying cosmological constant

In the cosmological constant dominated era at late times, Λ drives open and closed universes towards a flat universe, as usually expected. However, after some point the cosmological constant has decayed away sufficiently that matter dominates again. This causes models with positive spatial curvature ($\Omega > 1$) to slow down and then recollapse. The density parameter Ω of those models increases and diverges when $H = 0$ for finite values of the scale factor, and this leads to the emergence of cyclic universes. A closed universe will cycle through phases of expansion and collapse, and an open universe will expand forever, tending towards an empty universe. Again one should

note that there are models that exist for any measured $\Omega_{\text{Total}} > 0$ at the present day.

The fixed points are indicated by red-circled black dots: two centres $F1$, $F2$, and an Einstein static universe $E2$. The fixed points $F1$ and $F2$ have closed cycles around them, while the Einstein static universe $E2$ is a saddle point. The radii of curvature for the Einstein static universes in Figure 3 and Figure 5 is calculated below. By setting $H = 0$ in equations 2.11 and 2.12, one obtains

$$R_E = \Lambda_E^{-1/2} = \frac{1}{\sqrt{4\pi G\rho}}. \tag{2.21}$$

Using estimates for the inflationary potential energy and the current value of the cosmological constant of $\Lambda_{inf} \approx 10^{14} GeV$ and $\Lambda_{DE} \approx 10^{-12} GeV$, the radii of curvature are $R_{E1} \approx 10^{-7} GeV$ and $R_{E2} \approx 10^{6} GeV$. Thus if this model were modified to include a radiation dominated first stage, the first Einstein static universe (the source in the emergent universe scenario) would be much smaller than the second one (the static universe corresponding to the current value of dark matter).

The cyclic universes around $F1$ and $F2$ are not viable universe models, as they exclude the formative phases of the universe, such as inflation, reheating and recombination. However, the red curve shows a cyclic universe that exhibits a history like that of our universe after its collapse phase and bounce at $\Omega = \infty$. This illustrates the possible cyclic nature of our universe with the red bar representing our current position in its evolution. Although there is a cyclic model for every value of $\Omega_0 := \Omega(t_0) > 1$ in Figure 5, where t_0 is the present time, only those satisfying 2.1 and 2.2 will be compatible with current observations.

2.5.4 Time asymmetric universe with decaying cosmological constant

Previously it has been assumed that there is symmetry between the phases of expansion and collapse, but this is physically unrealistic, with progressive cycles in fact differing from each other. This was first indicated in the work of Tolman [45]. He introduced the presence of a viscous fluid in an attempt to describe a cyclic universe, finding that each successive cyclic phase will have progressively shorter periods and larger amplitudes because of entropy increase [45]. Barrow and Dabrowski [65] found an end to Tolman's growing cycles when introducing $\Lambda > 0$, and for any $\rho + 3p < 0$. Rees [66] then showed that astrophysical considerations would make the collapse phases differ from expansion phases, creating asymmetry. It has since been found that cosmological hysteresis — an asymmetry in the equation of state during expansion and collapse — causes an increase in amplitude of successive expansion cycles [54]. This applies to time-symmetric and non-dissipative governing equations, as has been used here, showing that this system can possess an arrow of time [53].

The following section focuses on the fact that the inflationary dynamics will not be time symmetric between the expansion and collapse phases because of the nature of inflationary dynamics.

2.6 Inflationary dynamics

The inflationary expansion phase is assumed to be that of a slow-roll field, as usual. The collapsing phase of inflation, however, needs further examination. One can ask, 'can this phase of inflation also be slow rolling?' and if so, 'will it remain reasonably spatially homogeneous so that one can continue to use a Robertson-Walker model for the geometry?' These questions are tackled in the sections to follow.

2.6.1 Inflationary fields

The Klein-Gordon equation for a spatially homogeneous field in a FLRW universe is

$$\ddot{\phi} + 3H\dot{\phi} = -V'(\phi). \tag{2.22}$$

The energy density is given

$$\rho = \dot{\phi}^2/2 + V(\phi) \tag{2.23}$$

and the pressure

$$p = \dot{\phi}^2/2 - V(\phi), \tag{2.24}$$

so one finds that w is given by

$$w = \frac{p}{\rho} = \frac{\dot{\phi}^2/2 - V(\phi)}{\dot{\phi}^2/2 + V(\phi)}. \tag{2.25}$$

Consider two different simple cases for the collapsing phase in the $k = +1$ models.

2.6.1.1 Flat potential

Suppose one has a flat potential;

$$\frac{\partial V(\phi)}{\partial \phi} = 0. \tag{2.26}$$

2.22 becomes

$$\ddot{\phi} = -3\frac{\dot{a}}{a}\dot{\phi} \Leftrightarrow \frac{d\log\dot{\phi}}{dt} = -3\frac{d\log a}{dt}. \tag{2.27}$$

Integrating this,

$$\log(\dot{\phi}/\dot{\phi}_0) = -3(\log(a/a_0)) \Rightarrow \dot{\phi}/\dot{\phi}_0 = (a/a_0)^{-3}, \tag{2.28}$$

and hence as $a \to 0$, $\dot{\phi} \to \infty$ and the solution becomes velocity dominated. It is represented by having the phase plane as before, except the collapsing inflaton dominated phase now (from 2.25) has equation of state $w = 1$. A singularity occurs. The solution is time asymmetric with no cyclic models except those around F2, which cannot represent the observed universe (Figure 6). All the observationally viable $k = +1$ models that reach a maximum and start contracting, collapse into a final singularity where $\Omega \to 1$ at a finite time in the future.

2.6.1.2 Quadratic potential

Next considered is a quadratic potential;

$$V(\phi) = \frac{m^2}{2}\phi^2. \tag{2.29}$$

Equation 2.22 becomes

$$\ddot{\phi} = -3\frac{\dot{a}}{a}\dot{\phi} - m^2\phi. \tag{2.30}$$

This gives a potential dominated solution, and hence equation of state $w = -1$ (from 2.25); a symmetric collapsing phase of inflation, leading to cyclic models.

The nature of inflation is highly sensitive to both the potential and the initial conditions. Due to the time reversal invariance of the underlying physics of the model, the set of collapsing cosmologies can be described as the reversal of the corresponding set of expanding solutions. This means that there are solutions that exhibit all possible realisations of w between -1 and 1 over the course of collapse. There are solutions which will exhibit strong potential domination, strong velocity domination and all cases in-between during collapse. Particularly, there will be solutions which have $w < -1/3$ at the point where $\frac{8\pi G\rho}{3} = \frac{1}{a^2}$ and these will undergo a bounce.

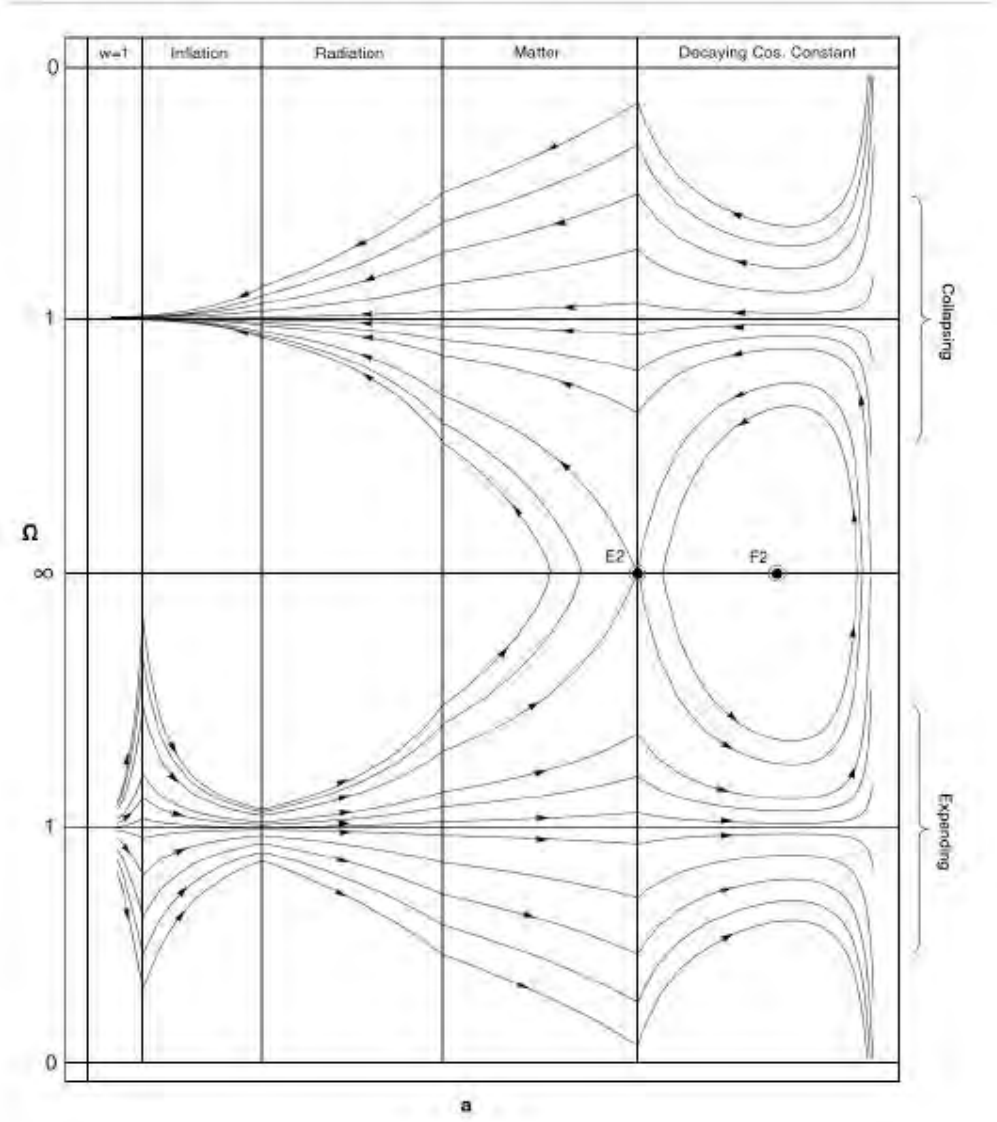

Figure 6: Phase plane with $p = \rho$ in collapse phase.

2.7 Chaotic cyclic cosmology

In the universe there exist small fluctuations about the Robertson-Walker geometry, however they are small enough that one can use this geometry in the model. One wishes to find whether the universe will remain reasonably spatially homogeneous during the collapse phase, so that one can continue to use a Robertson-Walker geometry.

2.7.1 Inhomogeneity growth

The growth of perturbations and matching perturbations at each cycle is a potentially problematic physical issue, as they may grow during the collapse phase, destroying the Robertson-Walker like state of the universe [49]. Thankfully this is not necessarily the case when one takes the inflationary equation of state into account.

In order to investigate the perturbation growth, one can use the linearised growth equation (38 in [67]) on the Friedmann equation with $w = p/\rho = const$ and $\Lambda = 0$. This 3+1 gauge invariant

and covariant formalism [67,68] centres on the comoving fractional spatial density gradient, defined as

$$\mathcal{D}_a := h^b_a \rho_{,b}/\rho \tag{2.31}$$

for an observer with 4-velocity u^a ($u_a u^a = -1$), where $h_{ab} := g_{ab} + u_a u_b$ projects orthogonal to u^a [69,70]. The result when used on the Friedmann equation is

$$\ddot{\mathcal{D}}_a = -(2-3w)H\,\dot{\mathcal{D}}_a + \left(\frac{(1-w)(1+3w)}{2}\kappa\rho\right)\mathcal{D}_a + w\frac{n^2}{a^2}\mathcal{D}_a. \tag{2.32}$$

The signs of the terms on the right hand side of this equation depend on the equation of state as in Table 1.

Source	**Term 1**	**Term 2**	**Term 3**
matter ($p = 0$, $w = 0$)	$-2H$	$\frac{1}{2}\kappa\rho$	0
radiation ($p = \rho/3$, $w = 1/3$)	$-H$	$\frac{2}{3}\kappa\rho$	$\frac{1}{3}\frac{n^2}{a^2}$
velocity dominated ($p = \rho$, $w = 1$)	$+H$	0	$\frac{n^2}{a^2}$
potential dominated ($p = -\rho$, $w = -1$)	$-H$	-2$\kappa\rho$	$-\frac{n^2}{a^2}$

Table 1: The terms in equation 2.32 for a variety of matter types. One can see that the first term retards structure growth during expansion ($H > 0$), acting as a friction force, but speeds it up during contraction ($H < 0$). However, the second term generates structure for ordinary matter and radiation, but causes oscillations for a cosmological constant, as does the third term.

During an inflationary collapse phase ($H < 0$), the first term soon dominates and is positive, and can make perturbations grow very fast, destroying the spatial homogeneity of the model. This is the inhomogeneity catastrophe envisaged by Penrose that may occur when collapse takes place [52]. Whether this occurs or not depends on the initial conditions, and thus they require careful consideration.

Note that there are related calculations on perturbation growth in some other cyclic models, e.g. [34–37], but they do not necessarily apply to this model, as here one has a singularity-free bounce, which is in contrast to the other models studied.

2.7.2 Chaotic cyclic models

Given the previous sections, one can plausibly claim that what occurs is equivalent to Linde's chaotic inflation [71–73], except now occurring during the collapse phase. During this phase, $\dot{a} < 0$, the fluctuations of the inflaton would result in some regions existing with $\dot{\phi}_0 > 0$ after the inflaton turns on, while in others $\dot{\phi}_0 < 0$. Considering this together with the cases explored in the previous section, one has:

- **Case I** In some regions, one will get a velocity dominated collapse to a singularity, locally, as in Figure 6.

- **Case II** In some regions with $\dot{\phi}_0 > 0$ one may get slow rolling and a potential dominated collapse phase;
- **Case IIA** In some of those cases inhomogeneity will build up, and the Robertson-Walker geometry will no longer apply; then the collapse phase will end up in many black holes;
- **Case IIB** In the other regions, one will get a potential dominated collapse to a minimum, followed by a bounce, locally, as in Figure 5.

The result is an inhomogeneous situation that consists of piecewise- singularities and bounces, leading to a chaotic inflation type scenario. Each cycle collapses into a mixture of singularities and bounces, and this can continue for many bounces. Although many regions of the universe will expand to a maximum before recollapsing into a singularity, some will collapse to a minimum and re-expand. Due to the nature of inflation, the latter regions will dominate the volume of the universe.

2.7.3 Quantum effects

In the standard case of chaotic inflation, quantum fluctuations can move up or down the potential. Assuming this holds in the case of collapsing inflation, the chaotic cyclic picture presented above is supported and even reinforced; some regions will get an even longer slow roll and others will get a stronger velocity dominated phase. The fluctuations, typically on the order of the Hubble scale, may alter a velocity dominated collapse into a potential dominated one and *vice versa*, however this will not change the overall picture, qualitatively.

2.8 Compatibility with current data and physical viability

The main interest of this model lies in its compatibility with current data, and thus this is expanded upon below. The physical viability of such a model is also explored.

2.8.1 Curvature

An absolute requirement for the viability of this model is that of positive curvature, $\Omega_k > 0$. Should the curvature be found to be negative, this model would be ruled out, however with our universe so incredibly close to flat, it may be a long while before either case can be confirmed. The best constraints on the curvature will come from combining the radial and angular diameter distances measured in the baryon acoustic oscillation (BAO) experiments [74]. There exist a number of future experiments planning to measure baryon acoustic oscillations, such as the Square Kilometer Array (SKA) project [75], the Canadian Hydrogen Intensity Mapping Experiment (CHIME) [76], and the Hydrogen Intensity and Real-time Analysis eXperiment (HIRAX) [77].

Cosmic invariance limits dark energy independent experiments at the $\sigma(\Omega_K) \simeq 10^{-3}$ level; for example the forecasts of [74] predict an accuracy of the geometrical determination of the curvature to be a relatively large $\sigma(\Omega_K) \sim 0.006$. This cosmic invariance is the unfortunate result of being able to observe only part of the universe at a particular time, making it difficult to infer measurements for the entire universe. BAO measurements could improve upon this constraint by an order of magnitude when assuming a model of dark energy. Thus, for both ΛCDM and for a simple model of dark energy, parameterised by the two equation of state parameters by $w(a) = w_0 + w_a(1-a)$, one expects constraints to improve to the order of a few $\times 10^{-4}$.

Although one is limited in determining the curvature of the universe, one may yet confirm a closed universe, a result that would prove to be very interesting and have impacts not only on this work, but on all early universe theories.

2.8.2 Dark energy decay

Another condition for the cyclic model is that dark energy, at some point, decays. Considering it as a non-interacting perfect fluid, the energy conservation is

$$\frac{d\rho_\Lambda}{dt} = -3(\rho_\Lambda + p_\Lambda)H = -3\rho_\Lambda(1+w)H \tag{2.33}$$

and so dark energy will decrease in the future provided that $w > -1$, a condition met by current constraints (2.3). Further, it is possible that dark energy may indeed be increasing now, but in the future will begin to decay. This is supported if dark energy is modelled by an effective scalar field, and so a potential exists for almost any given behaviour [78].

Another stipulation is that dark energy not only decrease, but decay fast enough such that baryonic matter ρ_b begins to dominate over the dark energy ρ_λ at some time in the future. Proposed here is an exponential decay, however any decay in which ρ_Λ decays faster than $1/a^3$ will also suffice. Limits can be placed on the parameters in the decay of dark energy used in this model (2.19), using its derivative and current constraints on the equation of state (2.3) to obtain $B = -0.18^{+0.255}_{-0.273}$. Considering the upper limit, matter will dominate over dark energy at $a \approx 48$. Note that the bounds, of course, also allow for $B = 0$ — a non-decaying constant.

2.8.3 Inflationary constraints

As previously discussed, one requires conditions for the inflaton to be potential dominated in order for a bounce to occur, and hence one requires a quadratic (or higher order) potential to fit the inflationary constraints of Planck, WMAP, BICEP, and other projects[3]. The strong bounds from the joint BICEP-KECK array of observations of the CMB [79] exclude the dynamics of a scalar field inflaton, but are in keeping with quartic potential fields or multi-field inflation [80, 81], either of which can lead to a bounce as they allow for $w < -1/3$.

2.8.4 Singularity theorems

There also exists an important condition that one must evade, courtesy of Guth et al. Their theorem states that the universe must have been singular [82], however this is based upon two restrictive assumptions: either that there is only expansion, or that the average expansion is positive $H_{av} > 0$. This model forgoes both axioms with a universe that undergoes time symmetric phases of expansion and collapse, giving an average expansion of $H_{av} = 0$, and therefore Guth's theorem need not apply.

2.8.5 Bounces

The bounce, of course, plays an integral role in cyclic models. As can be seen in [1], an inflation induced bounce is possible, and does not evoke any new physics. This is the proposed bounce for this model. Many other (more exotic) approaches also exist, for example Loop Quantum Cosmology (LQC) [38, 83], models of ekpyrosis [34] and the introduction of exotic matter, such as ghosts and phantoms.

[3]Quadratic potentials are somewhat disfavoured compared to higher order potentials, however this does not present any problems for the model as higher potentials can also lead to a bounce. A quadratic potential was chosen for convenience.

2.8.6 Decaying Λ

The most natural way to achieve a decaying cosmological constant is to introduce an arbitrarily small constant to the scalar field potential used for the inflaton to give the correct value for Λ. This field can then be coupled to any other matter in the system [84]. By introducing a coupling term between different fluids, one can alter their dynamics. Adding a transfer term to the evolution equations of coupled fluids, one obtains

$$\dot{\rho_i} + 3H(\rho_i + p_i) = \sum_j \gamma_{ij}, \tag{2.34}$$

where γ_{ij} is antisymmetric and models energy flow between fluids[4]. One can introduce a transfer term between the cosmological constant and dust such that the energy for Λ fade away into the dust field. Similarly, one could have the scalar field coupled to dust, and by introducing a $\gamma_{\Lambda d}$ (a function of H) have this occur only at late times. One can also model the energy to flow from the inflaton and into radiation. This can be done particularly neatly by having γ_{ij} contain a $\delta(w_1 - w_2)$, causing the inflaton to dump energy into radiation and dust etc as it descends on its potential. Considering the collapsing phase then, this creates a nice mechanism for returning energy to the inflaton from the radiation phase.

It should perhaps also be noted that with further investigation one may find that the the cosmological constant may in fact turn out to be a relic of early data surrounding Type Ia supernovae [85]. Should this be the case, cyclic models as envisioned here could exist without the need of a decay mechanism for the cosmological constant.

There are many interesting questions that remain in cyclic cosmology, such as entropy and perturbation growth, and the physics of the reheating process, and these are left for future exploration.

2.9 Discussion

The use of phase planes to model Friedmann's equations (although not encompassing the subtleties of the physics) provides a wonderfully visual means to explore cyclic models. The history of the universe is modelled using the cosmological density parameter Ω with respect to the rate of expansion a, while different values of w represent different epochs through which the universe has evolved. The phase plane analysis of [55] was updated to include the dark energy dominated epoch, considering two cases: a true and a decaying cosmological constant. In the former case the universe is found to expand forever, tending towards a flat universe. In the latter case, open universes expand forever, tending towards an empty universe, and closed universes become cyclic. This cyclic model is chaotic, with some regions re-collapsing into black holes and others bouncing before re-expanding. Note again that with a decaying cosmological constant and positive spatial curvature, no special mechanisms are needed to invoke a cosmic turnaround. Further, no new physics is needed at the bounce and the model is in keeping with current observations.

[4]Energy is conserved since γ is antisymmetric, and so the energy that leaves one field, enters another.

3 Kicking Chameleons

3.1 Introduction

In 2011, the Nobel Prize for physics was awarded jointly to Schmidt and Riess for observing the dimming of distant supernovae, implying that the universe is expanding at an accelerating rate. It is a well known conundrum that this phase of acceleration is not accounted for by the observed mass-energy of the universe. In fact, all data to date suggest that a new component of mass composing of 70% of the total energy budget of the universe is required to drive this expansion. The fact that we barely understand such a significant portion of our universe is astounding. Further more, we are so confident in our observations that despite our lack of understanding we have already awarded a Nobel Prize for this observation. Clearly there is a large gap we still need to fill, and to do this, we need to find a compelling candidate to explain this observation. In order to be sure that what we believe to be a cosmological effect is indeed coherent with our understanding of physics at all scales, this candidate should emerge from a theoretical framework that is built on fundamental physics, and ideally should be testable in complementary ways. A compelling candidate fulfilling these requirements comes in the form of Chameleon gravity, a scalar-tensor theory of gravity, as proposed in 2003 by Khoury and Weltman [61].

Chameleon theory considers the existence of a particle that couples conformally to matter. This scalar field ϕ, the Chameleon, has an effective potential that is the sum of its self-interaction term and an exponential term from the coupling. In order to be coherent with the confirmed predictions of Big Bang Nucleosynthesis (BBN), one requires this potential to be a minimum. This minimum depends on the local matter density, and so as a result the scalar field increases in mass with the local matter density.

In some cases one is required to consider the thermodynamic effects of the universe quite carefully in order to achieve this minimum. An example of such a case occurs when the field starts with a very large field value. In the radiation dominated phase of the early universe there is no force from matter to escort the effective potential to its required minimum. This result is, however, naive. As the universe expands, different matter species will briefly jump out of equilibrium with the background and so will contribute for a short while to the trace of the energy momentum tensor. This creates a restoring force on the Chameleon, known as a 'kick'. This process, until recently, was believed to be well-understood and explained by the Chameleon framework. It was however shown by Burrage et al. that some subtleties arise when the problem is considered in the Jordan frame [2, 3]. They found that in this frame and at a fixed temperature, the kicks push the field towards its potential minimum with a large velocity. This so-called 'surfing solution' leads to rapid variations in the scalar's mass and excitation of high energy-modes. These highly energetic quantum fluctuations invalidate any classical treatment of the Chameleon, suggesting that the Chameleon model cannot remain consistent in the very early universe unless the field is sufficiently weakly coupled to matter. This claim is explored and as a proposed solution, a DBI correction is added.

Section 3.2 is offered by means of introduction to Chameleon gravity and DBI corrections.

3.2 Background

3.2.1 Chameleon gravity

With the accelerated expansion of the universe, the need arises for a prominent cosmological constant Λ or some other dark energy candidate, one of which is the Chameleon.

The Chameleon is a scalar field that couples to matter, giving the scalar field a mass depending on the local density of the matter. High density regions in the universe mean a large field mass, whereas low density regions result in a small field mass. If a field is strongly coupled to matter, one expects to be able to see it as a 'fifth force', however no such evidence has yet been found. In terrestrial experiments, the large mass of the Chameleon suppresses its interactions with mass, making it hard to detect. Further, in observations of the Solar System, the action of the field is suppressed by a thin-shell mechanism. The aptly named Chameleon therefore cleverly evades detection, however there are numerous experiments designed to find it [86–88].

3.2.1.1 The action

The simplest Chameleon model is given by

$$S = \int d^4x\sqrt{-g}\left[\frac{M_{Pl}^2}{2}R - \frac{1}{2}(\partial\phi)^2 - V(\phi)\right] + S_m[\tilde{g}_{\mu\nu}, \psi], \tag{3.1}$$

where $\tilde{g}_{\mu\nu}$ =exp$(2\beta\phi/M_{Pl})g_{\mu\nu}$ and β is a dimensionless coupling constant. As a reference for scale, when $\beta \sim \mathcal{O}(1)$ the Chameleon couples to matter with gravitational strength.

3.2.1.2 Equation of motion

The equation of motion for the Chameleon is given by

$$\nabla^2\phi = V_{,\phi}(\phi) + \sum_i (1 - 3w_i)\frac{\beta_i}{M_{Pl}}\rho_i e^{(1-3w_i)\beta_i\phi/M_{pl}}. \tag{3.2}$$

More simply, one writes

$$\nabla^2\phi = V_{eff,\phi}(\phi), \tag{3.3}$$

with the effective potential;

$$V_{eff}(\phi) \equiv V(\phi) + \sum_i \rho_i e^{(1-3w_i)\beta_i\phi/M_{pl}}. \tag{3.4}$$

3.2.1.3 The potential and effective potential

One can see in 3.4 that the potential for the Chameleon consists of one part related to the field and another related to the density of the matter the Chameleon is coupled with. The bare potential $V(\phi)$ is chosen such that it can give rise to the cosmic acceleration today via the slow-roll mechanism, therefore requiring:

- $\lim_{\phi\Rightarrow 0} V(\phi) = \infty$,
- $V(\phi)$ is C^∞, bounded below and strictly decreasing,
- $V_{,\phi}(\phi)$ is strictly negative and increasing,
- $V_{,\phi\phi}(\phi)$ is strictly positive and decreasing.

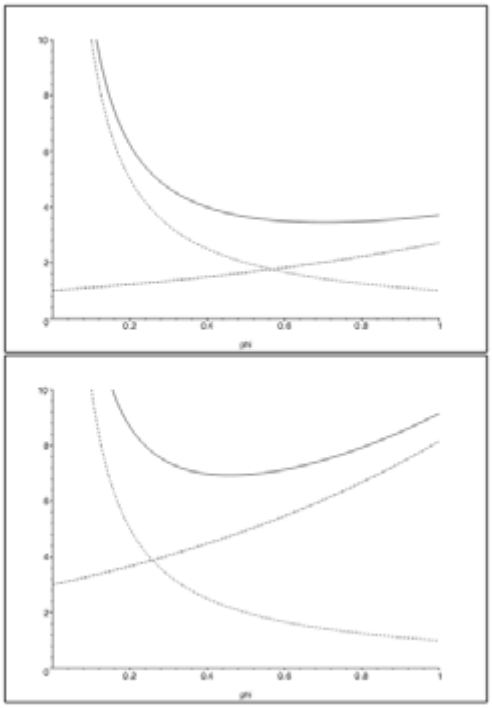

Figure 7: Figure 1 of [89]. $V(\phi) = \phi^{-1}$ (decreasing dotted line) and $\rho = 1$ and $\rho = 3$ in the first and second plot respectively. The effective potential in each case is shown by the solid line.

Plotting the constitutive parts of the effective potential provides a clear visual of the way in which the local matter density changes the effective potential of the Chameleon, as seen in Figure 7.

The most common potentials used are the inverse power-paw potential;

$$V(\phi) = \frac{M^{4+n}}{\phi^n}, \tag{3.5}$$

and the exponential potential;

$$V(\phi) = M^4 exp\Big(\frac{M^n}{\phi^n}\Big). \tag{3.6}$$

3.2.2 Dirac-Borne-Infeld (DBI) modification

A DBI modification is a UV correction for high energy physics. Since the temperatures in the very early universe were incredibly high, it is important that one recasts the Chameleon in this high energy regime, and prove that a consistent UV modification of the Chameleon action stabilises the field in the presence of the kicks.

At high energies, the DBI correction dynamically renormalises the coupling strength of the Chameleon such that it is weakly coupled to matter fields, and so suppresses the surfing behaviour. At low energies, such as in the late universe, the original Chameleon is recovered. This preserves the viability of the Chameleon on all scales without the need to constrain its coupling strength in general.

The DBI modification is in the form of derivative self interactions that cause the velocity term of the scalar fluctuations to pick up a factor Z to become $-\frac{1}{2}Z(\partial\delta\phi)^2$. Canonically normalising

the scalar fluctuation, it couples to the trace of the energy momentum tensor with a strength $\beta/\sqrt{Z}M_{Pl}$. Therefore, when derivative interactions dominate over the canonical kinetic term, the Z factor becomes large and the coupling to matter becomes weak.

The DBI generalisation of the Chameleon becomes

$$S = \int d^4x\sqrt{-g}\left[\frac{M_{Pl}^2}{2}R + \Lambda^4 - \Lambda^4\sqrt{1+\frac{(\partial\phi)^2}{\Lambda^4}} - V(\phi)\right] + S_m[\tilde{g}_{\mu\nu},\psi], \tag{3.7}$$

where Λ is the DBI correction. Expanding the action to the leading order with $(\partial\phi)^2 \ll \Lambda^4$ in the low energy limit, one recovers the original Chameleon action.

The coupling strength is determined by the γ-factor;

$$\gamma = \frac{1}{\sqrt{1+\frac{(\partial\phi)^2}{\Lambda^4}}}. \tag{3.8}$$

The larger the value of γ, the weaker the effective coupling. A weak coupling of the Chameleon to matter suppresses the excursions generated by the kick.

A DBI modification is shown in the following sections, through dynamical systems analysis and numerical simulations, to nullify the surfing behaviour of the Chameleon for sufficiently small Λ values, relative to the energy scale of the kick.

3.3 Surfing Chameleon

3.3.1 Obtaining the surfing solution

It is important to note that the kick Σ is the same when modelled in the Jordan-frame temperature and in the Einstein-frame temperature. This can be seen by looking at the expression for the kick in the Einstein frame;

$$\Sigma = \frac{\rho_{*R} - 3p_{*R}}{\rho_{*R}}, \tag{3.9}$$

where ρ and p the energy density and pressure of the radiation field, and noting that $\rho_* = e^{4\beta\phi/M_{Pl}}\tilde{\rho}$ and $p_* = e^{4\beta\phi/M_{Pl}}\tilde{p}$ [2,3].

In order to obtain the surfing solution, one should note that the Jordan frame temperature is given by

$$T_J[g_{*S}(T_J)]^{1/3} = [g_{*S}(T_{J,i})]^{1/3}T_{J,i}e^{\beta(\phi_i-\phi)/M_{Pl}}\frac{a_{*,i}}{a_*}. \tag{3.10}$$

One defines efolds $N \equiv \ln\frac{a}{a_{,i}}$ and rescale $\varphi \equiv \phi/M_{Pl}$ to obtain

$$T_J[g_{*S}(T_J)]^{1/3} = [g_{*S}(T_{J,i})]^{1/3}T_{J,i}e^{\beta(\varphi_i-\varphi)}e^{-N}. \tag{3.11}$$

An Ansatz for the surfing solution is given by

$$\varphi = \varphi_S - \frac{(p-p_S)}{\beta}. \tag{3.12}$$

Here p_S is the time at which the surfing behaviour begins and the field at this time has a value

$$\varphi_S = \varphi_i - \frac{p_s}{\beta} - \frac{\lambda}{\beta}, \tag{3.13}$$

where λ is a constant.

Inserting this solution into the expression for the Jordan-frame temperature, equation 3.11, one obtains

$$T_J[g_{*S}(T_J)]^{1/3} = T_{J,i}[g_{*S}(T_{J,i})]^{1/3}e^{\lambda}. \tag{3.14}$$

This implies that the Jordan frame temperature is constant while on the surfing solution.

The surfing solution has $\varphi'' = 0$ and $\varphi' = -1/\beta$, and consequently the kick function is

$$\Sigma(T_S) = \frac{2}{6\beta^2 - 1}, \tag{3.15}$$

while on the surfer.

3.3.2 Dynamical systems analysis

To begin, the standard Chameleon is analysed using dynamical systems to complement the results of [2,3]. This corresponds to the limit $\Lambda \to \infty$ to decouple the DBI derivative interactions.

The equations of motion for the Chameleon in flat FLRW cosmology (as derived in B.1) are

$$3M_{Pl}^2H^2 = \rho_\phi + \rho; \tag{3.16a}$$

$$M_{Pl}^2\left(2\dot{H} + 3H^2\right) = -p_\phi - p; \tag{3.16b}$$

$$\ddot{\phi} + 3H\dot{\phi} + V'(\phi) = -\frac{\beta}{M_{Pl}}\rho\Sigma; \tag{3.16c}$$

where $H = \dot{a}/a$ is the Hubble parameter, ρ and p the energy density and pressure of matter, and $\rho_\phi = \frac{\dot{\phi}^2}{2} + V$, $p_\phi = \frac{\dot{\phi}^2}{2} - V$, the energy density and pressure associated with the scalar field. As in [2,3], one denotes $\Sigma = (\rho - 3p)/\rho$, so that for a perfect fluid with equation of state $w = p/\rho$, one has $\Sigma = 1 - 3w$. Also as in [2,3], since the matter fields are the dominant source of the Chameleon's dynamics in the early universe, $V(\phi)$ is neglected.

Using 3.16a to eliminate ρ from the equations and using the fact that $p_\phi = \rho_\phi = \frac{\dot{\phi}^2}{2}$ when the potential is neglected, one is left with

$$M_{\rm Pl}^2H^2(4 - \Sigma) + 2M_{\rm Pl}^2\dot{H} + \frac{(2 + \Sigma)}{3}\rho_\phi = 0; \tag{3.17}$$

$$\ddot{\phi} + 3H\dot{\phi} + 3M_{\rm Pl}\beta\Sigma H^2\left(1 - \frac{\rho_\phi}{3M_{\rm Pl}^2H^2}\right) = 0. \tag{3.18}$$

For the analysis to follow, one can think of the surfer as a fixed line in an autonomous dynamical system with variables;

$$x = \beta\phi + M_{\rm Pl}\ln a; \tag{3.19}$$

$$y = \frac{\rho_\phi}{3M_{\rm Pl}^2H^2}; \tag{3.20}$$

$$z = \beta\dot{\phi} + M_{\rm Pl}H. \tag{3.21}$$

x is defined such that $\dot{x} = 0$ represents a constant Jordan frame temperature $T_J \propto e^{-\beta\phi/M_{\rm Pl}}/a$, the characteristic property of the surfer [2,3]. y is standard for fixed point analysis in cosmology and

gives the ratio between the energy density of ϕ and the critical density.

Recasting the Chameleon's system of equations in these variables;

$$\dot{x} = z, \tag{3.22}$$

$$\dot{y} = \frac{1}{H_y}\left[H_z\left(3Hz - \frac{1}{2}M_{\rm Pl}H^2(1-y)\left(2+\Sigma(1-6\beta^2)\right)\right) + \frac{H^2}{2}\left(\Sigma - 4 - y(\Sigma+2)\right)\right]; \tag{3.23}$$

$$\dot{z} = -3Hz + \frac{1}{2}M_{\rm Pl}H^2(1-y)\left(2+\Sigma(1-6\beta^2)\right); \tag{3.24}$$

where $H_y = \frac{\partial H}{\partial y}$, $H_z = \frac{\partial H}{\partial z}$ and $H(y,z)$ is given implicitly by the equation

$$M_{\rm Pl}^2H^2y = \frac{(z - M_{\rm Pl}H)^2}{6\beta^2}. \tag{3.25}$$

Explicitly solving for $H(y,z)$;

$$H(y,z) = \frac{z}{M_{\rm Pl}(1 \pm \sqrt{6\beta^2 y})}. \tag{3.26}$$

Assuming that the conformal coupling in the matter coupling decreases over time, $\frac{\beta\dot{\phi}}{M_{\rm Pl}} = \frac{z}{M_{\rm Pl}} - H < 0$, and one takes the lower root in 3.26. For $y \neq 1/6\beta^2$, the fixed points of this system have $z = 0$, with x and y arbitrary constants. This corresponds to an empty universe in which fixed points always have $H = 0$. Conversely, when $y = 1/6\beta^2$, fixed points have $z = 0$ with x an arbitrary constant and no constraint on H.

The surfer is given by the latterly described line of fixed points at the critical value of Σ. These points have constant Jordan frame temperature $\dot{x} = 0$ and can exist at any H, provided Σ passes through $2/(6\beta^2 - 1)$.

Equations 3.22-3.25 are solved numerically for an array of initial conditions, with the trajectories of these solutions in the (H, z) plane plotted in Figure 8. When one has $\Sigma = 2/(6\beta^2 - 1)$, simulations confirm that for a large range of initial conditions the solutions are attracted to the surfing solution at $z = 0$.

For the interested reader, the action of the Chameleon is perturbed in B.2 and the Chameleon is found to be stable.

3.4 DBI correction

In this section it demonstrated how the DBI-Chameleon model eliminates the surfing behaviour for a natural choice of the scale of modification Λ. The analysis consists of idealised dynamical systems and numerical simulations.

3.4.1 Dynamical system analysis

Introducing $P(X) = \Lambda^4 - \Lambda^4\sqrt{1 - \frac{2X}{\Lambda^4}}$, where $X = -(\partial\phi)^2/2$, the following DBI modified field equations become

$$3M_{\rm Pl}^2H^2 = \rho_\phi + \rho; \tag{3.27}$$

$$M_{\rm Pl}^2\left(2\dot{H} + 3H^2\right) = -p_\phi - p; \tag{3.28}$$

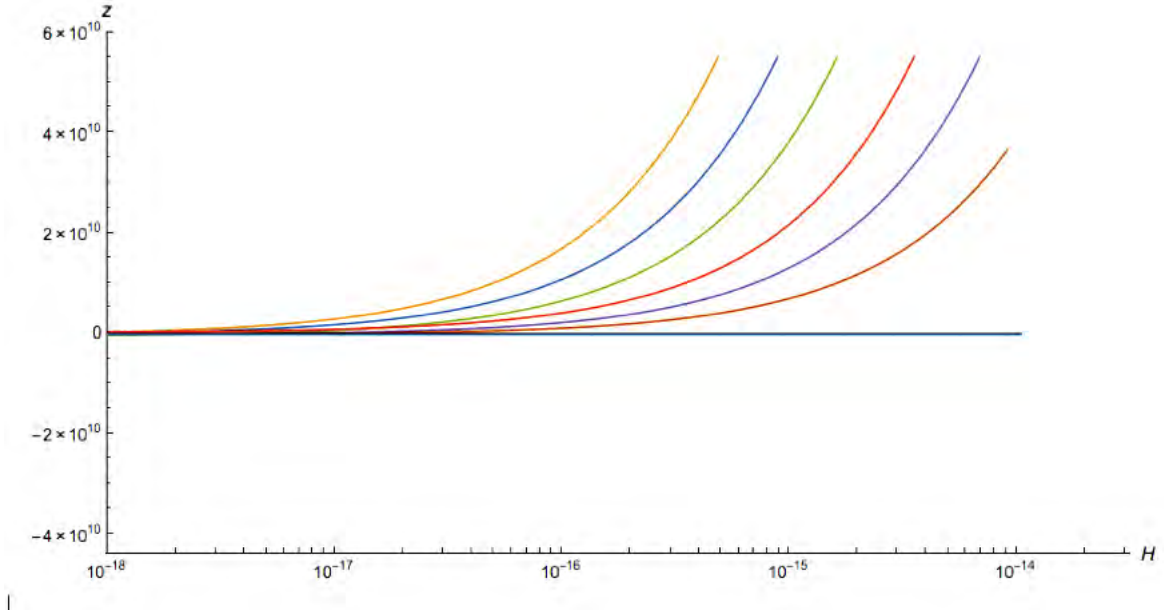

Figure 8: z against H for a range of initial conditions, indicated by different colours. $\Sigma = \dfrac{2}{6\beta^2 - 1}$; $\beta = 3$.

$$(P_{,X} + 2XP_{,XX})\,\ddot{\phi} + 3HP_{,X}\,\dot{\phi} + V'(\phi) = -\frac{\beta}{M_{\rm Pl}}\rho\Sigma; \tag{3.29}$$

where $P_{,X}$ denotes differentiation of $P(X)$ with respect to X. The energy density and pressure of the scalar now take a more complicated form of $\rho_\phi = 2XP_{,X} - P(X)$ and $p_\phi = P(X)$. Again assumed is a perfect fluid with the equation of state $w = p/\rho$ as the matter content, so that $\Sigma = 1 - 3w$, and the potential $V(\phi)$ is neglected. As a consistency check, by taking the limit $\Lambda \to \infty$, one recovers the standard Chameleon case. Again one eliminates ρ using 3.27 to obtain

$$M_{\rm Pl}^2 H^2(4 - \Sigma) + 2M_{\rm Pl}^2\dot{H} + p_\phi - \rho_\phi + \frac{(2+\Sigma)}{3}\rho_\phi = 0, \tag{3.30}$$

$$(P_{,X} + 2XP_{,XX})\,\ddot{\phi} + 3HP_{,X}\,\dot{\phi} + 3M_{\rm Pl}\beta\Sigma H^2\left(1 - \frac{\rho_\phi}{3M_{\rm Pl}^2H^2}\right) = 0. \tag{3.31}$$

Introducing the same set of variables as previously 3.19 - 3.21, one arrives at the following autonomous system;

$$\dot{x} = z; \tag{3.32}$$

$$\dot{y} = \frac{1}{H_y}\left[H_z\left(3Hs^2z - \frac{1}{2}M_{\rm Pl}H^2\left[(1-y)\left(2 + \Sigma(1 - 6\beta^2s^3)\right) + 3y(1-s) - 6(1-s^2)\right]\right) + \frac{H^2}{2}\left(\Sigma - 4 - y(\Sigma+2) + 3y(1-s)\right)\right]; \tag{3.33}$$

$$\dot{z} = -3Hs^2z + \frac{1}{2}M_{\rm Pl}H^2\left[(1-y)\left(2 + \Sigma(1 - 6\beta^2s^3)\right) + 3y(1-s) - 6(1-s^2)\right]; \tag{3.34}$$

where $s = \sqrt{1 - \dfrac{(z - M_{\rm Pl}H)^2}{\beta^2\Lambda^4}}$. Again $H_y = \frac{\partial H}{\partial y}$, $H_z = \frac{\partial H}{\partial z}$ but now $H(y,z)$ is given implicitly by the following equation;

$$\left(\Lambda^4 - \frac{(z - M_{\rm Pl}H)^2}{\beta^2}\right)\left(1 + \frac{3M_{\rm Pl}^2H^2y}{\Lambda^4}\right)^2 = \Lambda^4. \tag{3.35}$$

Analogous to the previous case, one requires that $z = 0$ with y chosen such that 3.35 does not constrain H. Setting $z = 0$ in 3.35, leads to the polynomial in $M_{\rm Pl}H$ given by

$$\left(\frac{9y^2}{\beta^2\Lambda^8}\right)(M_{\rm Pl}H)^6 + \left(\frac{6y}{\beta^2\Lambda^4} - \frac{9y^2}{\Lambda^4}\right)(M_{\rm Pl}H)^4 + \left(\frac{1}{\beta^2} - 6y\right)(M_{\rm Pl}H)^2 = 0. \tag{3.36}$$

The only way in which this does not constrain H is if, and only if, all of the coefficients vanish. This can be achieved in two ways. The first is to take $\Lambda \to \infty$ and set $y = 1/6\beta^2$, which gives the decoupled DBI interaction limit and hence the original Chameleon result. The second is to take $\beta \to \infty$, and set $y = 0$. In this limit, scalar fields are strongly coupled to matter and hence the surfer (originating from dominant matter kicks) re-emerges.

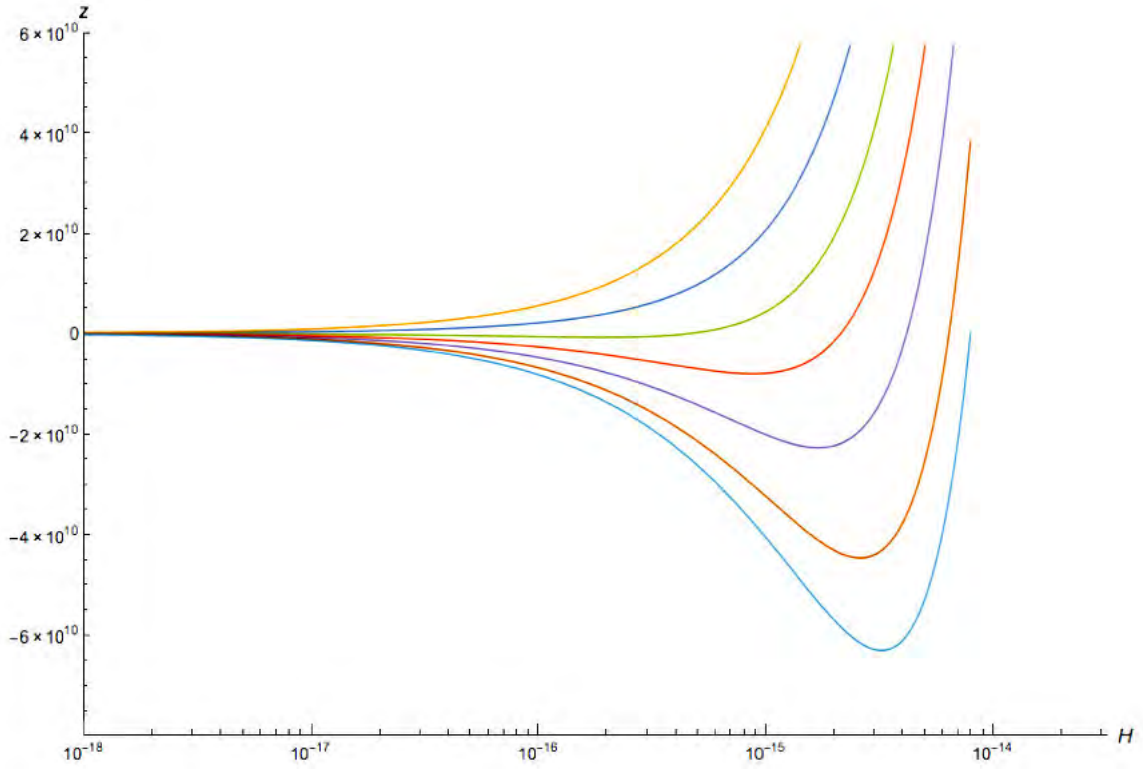

Figure 9: z against H for a range of initial conditions with a DBI-modification, indicated by different colours. $\Sigma = \dfrac{2}{6\beta^2 - 1}$; $\beta = 3$.

In general, one expects that the surfing behaviour of the Chameleon will be destroyed provided that $\Lambda^2 \lesssim M_{\rm Pl}H/\beta$, where the scale $M_{\rm Pl}H$ is set by the scale at which the kicks occur. This follows from the fact that the DBI corrections become significant whenever $\dot{\phi}^2 \sim \Lambda^4$ and on a surfer one has $\dot{\phi} = -M_{\rm Pl}H/\beta$.

Solving the dynamical system numerically, one can demonstrate the above. One can verify that in the limits when either $\Lambda \to \infty$ or $\beta \to \infty$, the surfer emerges. The image is like that of Figure 8, with all solutions approaching the surfing solution. One can also plot a DBI system, Figure 9, where β is of order 1 and $H \gtrsim \Lambda^2/M_{\rm Pl}$. One can see that the stable line at $z = 0$ that existed in the non-DBI case (Figure 8) is no longer present until the Hubble parameter H drops below the critical value set by $\Lambda^2/M_{\rm Pl}$. This means that the surfer is not an attractor in the theory at high energy scales, and hence the surfing behaviour is destroyed.

3.4.2 Field excursions

Without the Chameleon surfing in the appropriate limit of the DBI modification, one expects the problematic field excursions preformed prior to BBN to be suppressed. This is essential in order to prevent the scalar field from hitting the potential at too high a velocity, causing the production of high energy quanta. The change in Jordan frame temperature gives a good estimation of the maximum field excursive undertaken by a Chameleon. While surfing, and neglecting the potential, the Jordan frame temperature is constant. This results in an (over-estimated) infinite field excursion, which tells one that the field shoots up the potential wall at too high a pace and much too early, causing a breakdown in classical Einstein Field Theory (EFT).

To compute the field excursions, note that

$$\Delta\phi = \int_{t_i}^{t_i+\Delta t} \dot{\phi}\, \mathrm{d}t, \tag{3.37}$$

where the kick remains close to the critical value between times t_i and $t_i + \Delta t$. "Close" here is defined in terms of the Jordan frame temperature as

$$\frac{\Delta T_J}{T_J} = -\int_{t_i}^{t_i+\Delta t} \frac{z}{M_p}\, \mathrm{d}t \leq |1|. \tag{3.38}$$

The maximum field excursions will result when the field is initially surfing, $z(t_i) = 0$, and therefore when $\dot{\phi}(t_i) = -M_{\rm Pl}H/\beta$. From this it follows that

$$\frac{\Delta\phi}{M_{p1}} \approx -\frac{H\Delta t}{\beta}. \tag{3.39}$$

Further, $z(t) \approx \dot{z}(t_i)(t - t_i)$, leading to

$$\frac{\Delta T_J}{T_J} \approx -\frac{\dot{z}(t_i)}{M_p}\frac{\Delta t^2}{2}. \tag{3.40}$$

Setting $z = 0$, $y \sim \mathcal{O}(1)$, and $\Sigma = 2/(6\beta^2 - 1)$ in equation 3.34 yields $\dot{z}(t_i) \sim \mathcal{O}(1)M_{\rm Pl}^3 H^4/\beta^2\Lambda^4$. Finally one obtains

$$\frac{\Delta\phi}{M_p} \approx \mathcal{O}(1)\frac{\Lambda^2}{M_{\rm Pl}H}\sqrt{\left|\frac{\Delta T_J}{T_J}\right|} \lesssim \frac{\Lambda^2}{M_{\rm Pl}H}. \tag{3.41}$$

The above equation is wonderfully illustrative, showing that Λ serves to suppress the large field excursions. Constraints on the variation of particle masses from BBN until the present suggests that one impose an upper bound $|\Delta\phi|/M_{\rm Pl} \lesssim 0.1/\beta$ [64]. Since the last and the most significant kick is due to the electron (at which point $M_{\rm Pl}H \sim (\mathrm{MeV})^2$) this requires that one takes $\Lambda \lesssim \mathrm{MeV}/\sqrt{\beta}$ to protect the theory from dangerously large field excursions.

3.4.3 Numerical simulations

Next the results of the dynamical systems analysis are confirmed by performing numerical simulations. The system is solved with realistic initial conditions and in the presence of a simplified kick. As was done in [2, 3], a change of variables is made to ones more suited to numerical simulation. This is achieved by rescaling the field ϕ by M_{Pl} and changing the time variable to Einstein frame efolds N. The equations of motion for the original Chameleon theory (3.17 and 3.18) become

$$2\frac{H'}{H} + (4 - \Sigma) + \left(\frac{2+\Sigma}{3}\right)\frac{\varphi'^2}{2} = 0; \tag{3.42}$$

$$\varphi'' + \left(\frac{H'}{H} + 3\right)\varphi' + 3\beta\Sigma\left(1 - \frac{\varphi'^2}{6}\right) = 0; \tag{3.43}$$

where in this section a prime denotes differentiation with respect to N. Similarly, the equations of motion for the DBI-Chameleon (3.30 and 3.31) become

$$2\frac{H'}{H} + (4-\Sigma) + \left[p_\phi - \rho_\phi + \left(\frac{2+\Sigma}{3}\right)\rho_\phi\right]/M_{\rm Pl}^2 H^2 = 0, \tag{3.44}$$

$$\left(P_{,X} + P_{,XX}\, M_{\rm Pl}^2 H'^2 \varphi'^2\right)\left(\varphi'' + \frac{H'}{H}\varphi'\right) + 3P_{,X}\,\varphi' + 3\beta\Sigma\left(1 - \frac{\rho_\phi}{3M_{\rm Pl}^2 H^2}\right) = 0. \tag{3.45}$$

For simplicity, a kick is approximated as a single Gaussian bump in terms of Jordan frame temperature such that

$$\Sigma(T_J) = A\exp\left[-\frac{(\log T_J - \log T_{peak})^2}{\sigma^2}\right]. \tag{3.46}$$

This is more realistic than a constant kick and so better represents the physical situation. The parameters A, T_{peak} and σ characterise the kick and are appropriately chosen to model the desired kick in [3]. For the purpose of this thesis, the electron/positron kick is concentrated one. This is the last and the most significant kick. This requires that one set $A = 0.1$, $T_{peak} = 2\times10^{-4}$ GeV and $\sigma = 0.3$. Since the Jordan frame temperature goes like $T_J \sim 1/a_J$ one can relate it to Einstein frame efolds by

$$T_J(N) = T_{J,i}\exp\left[-N - \beta\Delta\varphi(N)\right], \tag{3.47}$$

where $T_{J,i}$ is the initial Jordan frame temperature corresponding to $N = 0$ and $\Delta\varphi(N) = \varphi(N) - \varphi_i$ is the field excursion after N Einstein frame efolds. Combining 3.46 and 3.47 one gets an expression for the kick function in terms of Einstein frame efolds $\Sigma(N)$, which is used in the simulations.

The evolution equations 3.42, 3.43 and 3.44, 3.45 are solved with the Gaussian kick function 3.46. In the DBI-Chameleon simulations various values of Λ are used to demonstrate the effect of the DBI correction on the surfing solution. These are consistently compared and contrasted with the standard Chameleon by matching the initial conditions for ϕ and $\dot\phi$ in each case. In all simulations the matter coupling strength is chosen to be $\beta = 3$ and the initial Jordan frame temperature to be $T_{J,i} = 10^{-2}$GeV, approximately the temperature at which the electron/positron kick starts. The positive and negative $\dot\phi$ are investigated and their energy scale related to that of the kick by

$$\dot\phi_i = \Lambda_k^2\{0.8, -0.8\}, \tag{3.48}$$

with the energy scale of the kick $\Lambda_k = 10T_{peak} = 2\times10^{-3}$GeV. When $\Lambda \approx \Lambda_k$, $\dot\phi$ is strongly in the DBI regime, with $\gamma \approx 1.7$. It is therefore expected that the surfer no longer exists for these conditions. Neglecting any contribution to the energy density from non-relativistic matter, the initial energy density ρ_i is dominated by radiation and is given by

$$\rho_{r,i} = \frac{\pi^2}{30}g_*(T_{J,i})\,T_{J,i}^4 e^{4\beta\varphi_i}, \tag{3.49}$$

with $g_*(T_{J,i}) = 10.75$. This closes the system of equations and allows one to calculate the three initial conditions $\varphi_i, \varphi_i', H_i$. From this one can solve the required 3.42 and 3.43 or 3.44 and 3.45.

For the DBI-Chameleon, five runs are performed which correspond to values of Λ ranging from Λ_k to $10\Lambda_k$. The results are shown in Figures 10-12, where in each case one can see that as $\Lambda \to \Lambda_k$ the surfing solution becomes unstable and the attractor behaviour is destroyed. Note that

for these runs, the trajectories for the positive and negative $\dot{\phi}_i$ are very similar, and so only the positive are shown. In all of the simulations the thick black dotted line corresponds to the original Chameleon without DBI correction, grey broken lines (dashed, dot-dashed and dotted) correspond to Chameleons with DBI correction that do surf and solid lines correspond to Chameleons for which the DBI correction effectively destroys surfing behaviour. All curves represent 15 Einstein frame efolds.

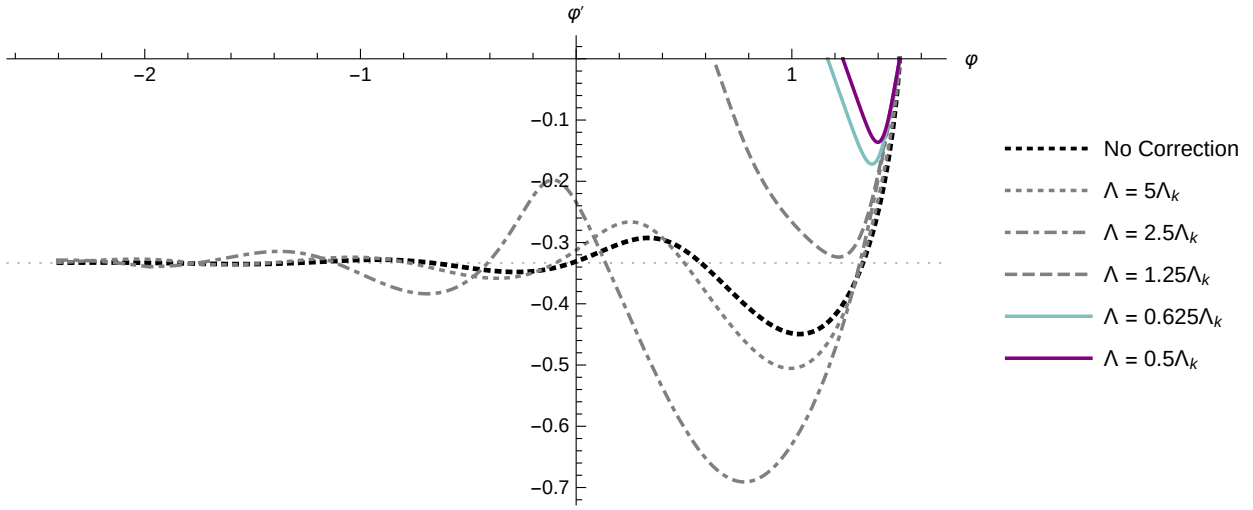

Figure 10: Phase diagram for φ' vs. φ. Dotted light grey line indicates the surfing solution at $-1/\beta$.

Figure 10 shows the trajectories in the $\varphi - \varphi'$ plane with the horizontal dotted grey line indicating the surfing solution at $-1/\beta$. The effect of the DBI correction is evident in the two solid coloured curves, where the field velocity decays to zero. In contrast, all other trajectories approach $-1/\beta$.

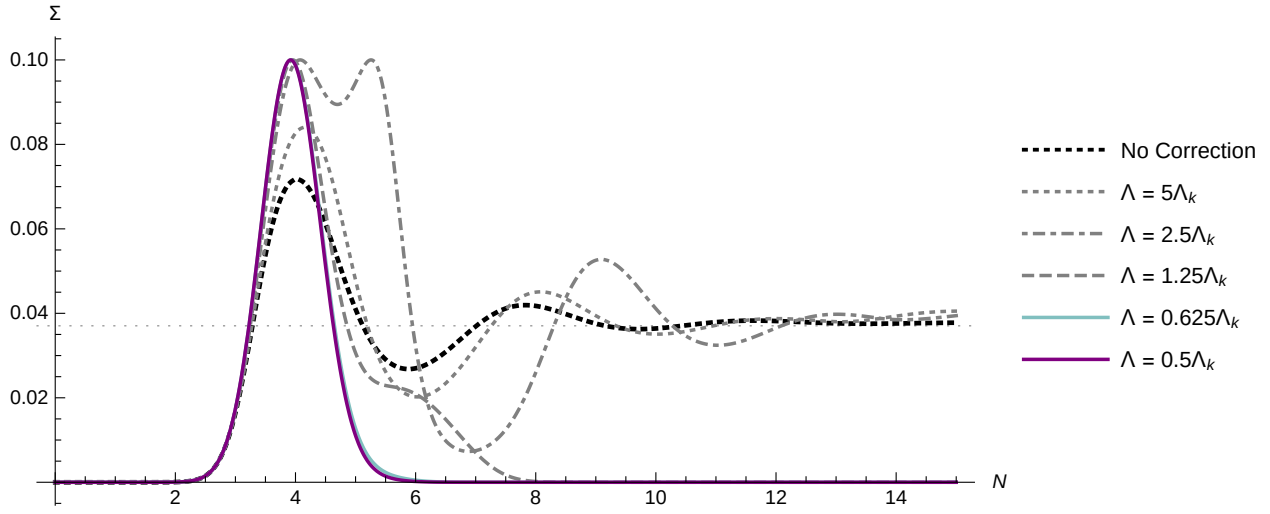

Figure 11: The kick as a function of Einstein frame efolds. Dotted light grey line indicates $2/(6\beta^2 - 1)$, the critical value of the kick at which the surf occurs. Chameleons that surf see a constant kick at this value.

Figure 11 shows the kick as a function of Einstein frame efolds with the horizontal dotted grey

line indicating the critical value at which the surf occurs, $\Sigma = 2/(6\beta^2 - 1)$. Chameleons which surf see an almost constant kick at this value, whereas the Chameleons in the DBI regime for which the correction is effective see a kick over a finite amount of Einstein frame efolds.

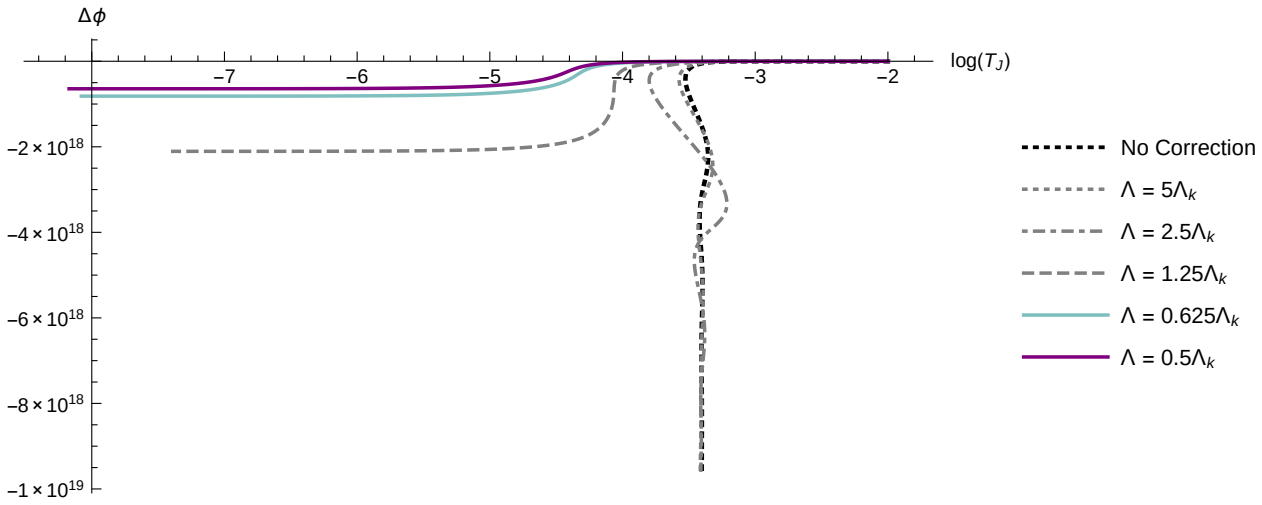

Figure 12: Field excursion vs. Jordan frame temperature.

Figure 12 shows the field excursion against Jordan frame temperature. The vertical line indicates the critical temperature of the surf, T_J^c. The solid coloured lines show the effect of the DBI correction on the field excursion, with stronger corrections reducing the excursion in the field.

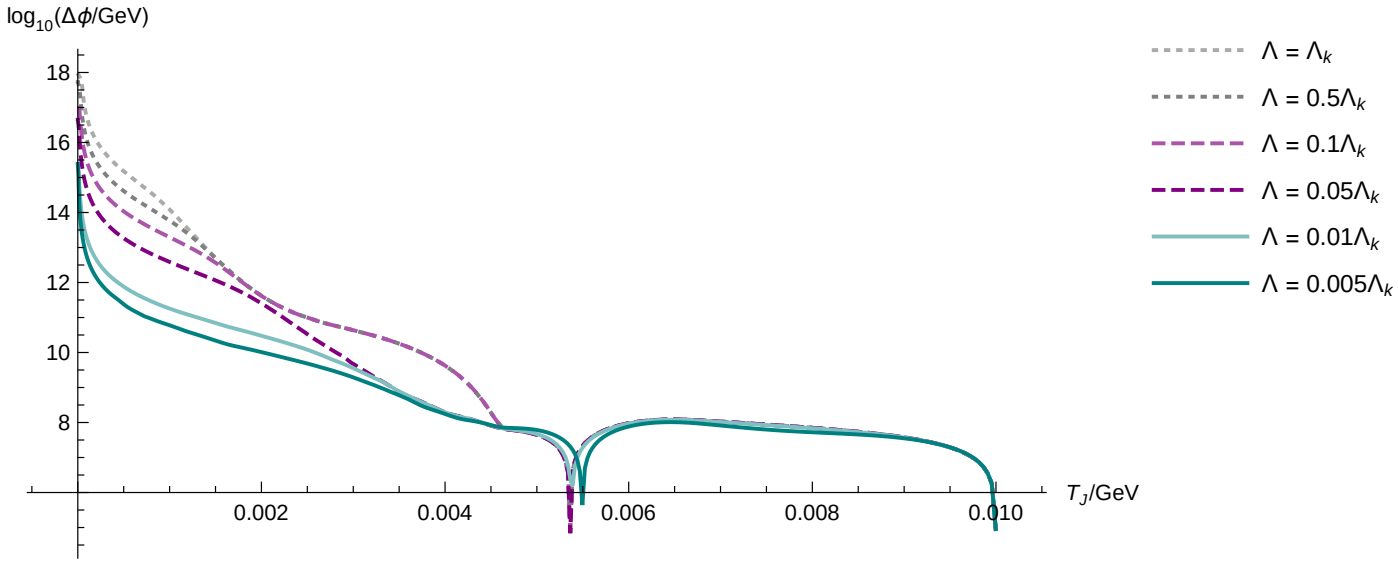

Figure 13: Field excursions vs Jordan frame temperature for variations in the DBI scale at fixed initial field velocity.

Although it is clear that the surfing behaviour is ultimately eliminated by the DBI correction, one might still worry that Planckian field excursions are still possible. These excursions would be problematic because if one imposes the BBN bound $\phi < 0.1 M_{pl}/\beta$ just before the electron kick, it would mean the scalar still crashes into the minimum of the effective potential during BBN with too

large a velocity. However, it is important to realise that these plots represent a worst case scenario, with the DBI scale close to the kick scale and the initial speed of the Chameleon close to the speed limit. One can easily suppress the field excursions to safe values by lowering the DBI scale by just an order of magnitude further. This is demonstrated in Figures 13 and 14. In Figure 13, the initial field velocity is held fixed for each run, whilst the DBI scale is lowered. This means the γ factor is increasing, and so the effective coupling is being weakened, suppressing the excursions generated by the kick. In Figure 14 the DBI scale and the initial velocity are lowered in tandem, such that the γ factor is held fixed. This time the effective coupling is unchanged between runs, but the field excursions are suppressed due to the decreasing initial velocity. This reflects the ability of the DBI structure to impose a cosmic speed limit on the scalar field. The Chameleon is therefore fully protected from hitting the potential in any catastrophic way.

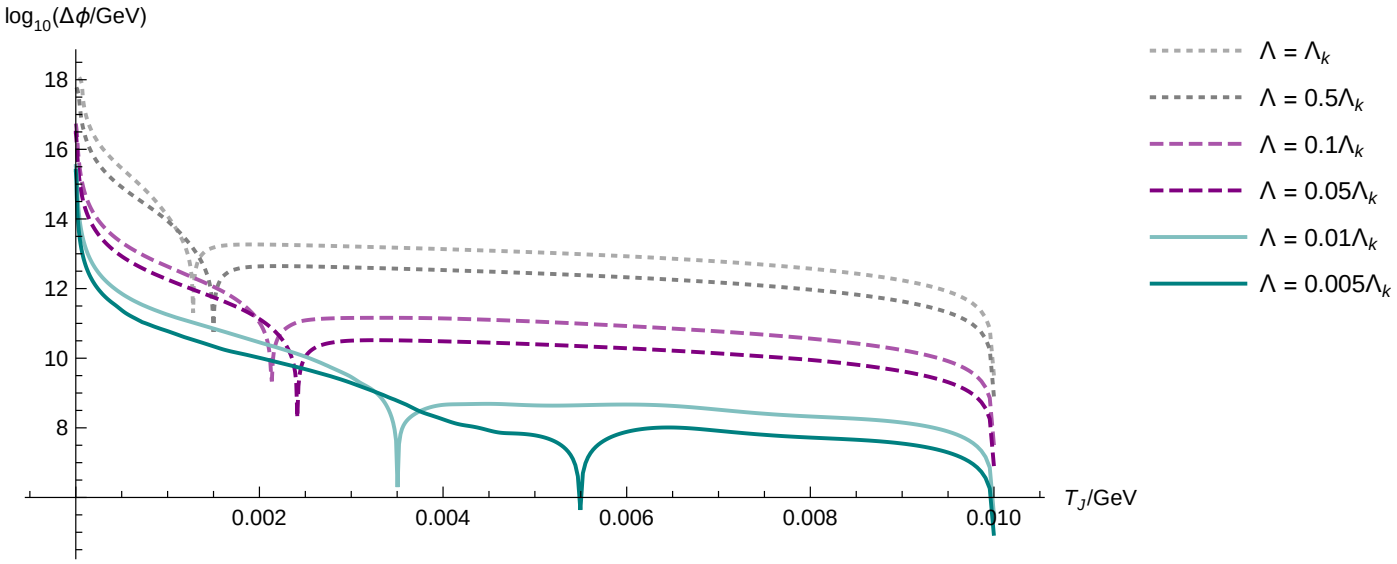

Figure 14: Field excursions vs Jordan frame temperature for variations in the DBI scale and the initial field velocity, holding the initial effective coupling fixed.

3.5 Discussion

The authors of [2,3] claim that for some set of initial conditions, the Chameleon is not a consistent classical field theory for describing the early universe. It appears that the previously thought-to-be understood process that escorts the Chameleon down the potential has catastrophic consequences. The kicks to the scalar caused by massive particles becoming non-relativistic during the radiation dominated era appear to cause significant field excursions leading to the production of highly energetic quantum fluctuations. These invalidate any classical treatment of the Chameleon, suggesting that the Chameleon must have been sufficiently weakly coupled to matter prior to BBN in order to remain consistent.

Considering Chameleon theory as an EFT with a DBI modification, it has been found that the scalar is protected from dangerously large field excursions. The DBI correction ensures that the Chameleon's effective coupling to matter is weakened dynamically in the early universe, causing the impact of the kicks to be suppressed. The mechanism by which this is achieved exploits derivative self interactions of the scalar in order to induce a large Z factor, thereby dominating the dynamics

as particles become non-relativistic for suitably chosen parameters:

$$\frac{(\mathrm{MeV})^2}{M_{\mathrm{Pl}}} \ll \Lambda \lesssim \frac{\mathrm{MeV}}{\sqrt{\beta}}. \tag{3.50}$$

Further, the DBI can be reduced to just an order of magnitude below the scale of the final kick in order to keep field excursions sub-Planckian. This ensures that the Chameleon will avoid crashing into the minimum of the effective potential during BBN and hence the DBI Chameleon will generically avoid the breakdown described in [2, 3].

4 Conclusion

Through analysing two very different systems, it is apparent that phase planes form an essential part of theoretical cosmology. In Section 2 the technique is used to demonstrate a cyclic universe model that is in keeping with current observations. The model is found to be chaotic in nature and relies on only two conditions; that the universe is open and that dark energy decays at some time in the future. Neither of these requirements have been confirmed nor ruled out by current observations, with the former perhaps impossible to verify within the foreseeable future.

The portraits are created using Friedmann's equations and are complemented with theory to account for physics that the dynamical system itself does not encompass. The perturbation growth during the collapsing phase of inflation is examined to find that a chaotic situation occurs, in which some regions of the universe collapse into singularities, and others bounce and re-expand. This depends on whether the collapse of the space is velocity- or potential dominated, respectively. Additionally, perturbation growth causes some potential dominated regions to collapse, too. Quantum fluctuations may cause a velocity dominated region to become potential dominated, and *vice versa*, however this does not change the dynamics overall.

In Section 3, the claims in [2, 3] that in the very early universe the Chameleon model is inconsistent unless significant restraints are placed on the coupling strength of the Chameleon to matter, are rebuked. To do this, a DBI modification is added to the equation of motion that describes the Chameleon and verifies the results through a dynamical systems analysis and numerical simulations. This UV correction serves to consider the Chameleon in the high energy regime, as it should be in the very early universe. The energy scale decreases as the universe expands, and eventually the equation of motion for the Chameleon reduces to its original form, as one observes it today.

The dynamical systems analysis shows that with a DBI modification the surfer is no longer an attractor, suggesting that the surfing behaviour of the Chameleon is destroyed. This is confirmed through a number of numerical simulations. Further, the excursions of the Chameleon in the DBI limit are confirmed to be sub-Plankian, ensuring that the Chameleon is in no danger of hitting the potential with speed. Chameleon gravity therefore remains a consistent model in the very early universe, with a DBI correction dynamically renormalising the coupling strength of the Chameleon to matter at high energies.

Cosmology is a vast field, covering the most fundamental of life's questions. With every paper published and every theory refuted or confirmed, cosmologists come slowly closer to answering these questions.

5 Acknowledgements

Thank you firstly to my primary supervisor and role model, Prof. Amanda Weltman. Not only has she guided me in my work and provided me with amazing opportunities, but she has helped me through the many challenges and difficulties in life with immense kindness and understanding. Thank you to Prof. George F.R. Ellis, my second supervisor and a legend in the field, for his support, his words of wisdom and the opportunities he has given me. Thank you to my mum and brother for their unconditional love and support.

Thank you also to Tony Walters and the Nottingham team; Dr Tony Padilla, Toby Wilson and David Stefanyszyn, for the collaboration of [4]. Thank you to Dr Jonathon Shock for his help with numerics. Thank you to Prof. Pedro Ferriera for a key remark on [1] and to Dr David Sloan for his work in [1].

Thank you finally to my amazing proofreaders; Duncan Greaves, Bridget Witts-Hewinson and Ashleigh Davies.

References

[1] G. F. R. Ellis, E. Platts, D. Sloan, and A. Weltman, "Current observations with a decaying cosmological constant allow for chaotic cyclic cosmology," 2015.

[2] A. L. Erickcek, N. Barnaby, C. Burrage, and Z. Huang, "Chameleons in the Early Universe: Kicks, Rebounds, and Particle Production," *Phys. Rev.*, vol. D89, no. 8, p. 084074, 2014.

[3] A. L. Erickcek, N. Barnaby, C. Burrage, and Z. Huang, "Catastrophic Consequences of Kicking the Chameleon," *Phys. Rev. Lett.*, vol. 110, p. 171101, 2013.

[4] A. Padilla, E. Platts, D. Stefanyszyn, A. Walters, A. Weltman, and T. Wilson, "How to Avoid a Swift Kick in the Chameleons," 2015.

[5] A. Einstein, "Cosmological Considerations in the General Theory of Relativity," *Sitzungsber. Preuss. Akad. Wiss. Berlin (Math. Phys.)*, vol. 1917, pp. 142–152, 1917.

[6] A. Freidmann, "Über die krümmung des raumes," *Zeitschrift für Physik*, vol. 10, pp. 377–386, 1922.

[7] E. Hubble, "A relation between distance and radial velocity among extra-galactic nebulae," *Proc. Nat. Acad. Sci.*, vol. 15, pp. 168–173, 1929.

[8] G. Lemaitre, "A homogeneous Universe of constant mass and growing radius accounting for the radial velocity of extragalactic nebulae," *Annales Soc. Sci. Brux. Ser. I Sci. Math. Astron. Phys.*, vol. A47, pp. 49–59, 1927.

[9] G. F. Smoot, "Cosmic Background Explorer (COBE) observations: New sky maps of the early universe," in *Electroweak interactions and unified theories. Proceedings, Leptonic Session of the 26th Rencontre de Moriond, Les Arcs, France, March 11-17, 1991*, pp. 167–181, 1991.

[10] H. Peiris, *WMAP First Year Results: Cosmological parameters and implications for inflation.* PhD thesis, Princeton U., 2003.

[11] P. A. R. Ade *et al.*, "Planck 2015 results. XIII. Cosmological parameters," 2015.

[12] M. Colless, "First results from the 2dF galaxy redshift survey," *Phil. Trans. Roy. Soc. Lond.*, vol. A357, p. 105, 1999.

[13] J. E. Gunn and D. H. Weinberg, "The Sloan digital sky survey," 1994.

[14] A. G. Riess *et al.*, "Observational evidence from supernovae for an accelerating universe and a cosmological constant," *Astron. J.*, vol. 116, pp. 1009–1038, 1998.

[15] D. Maoz, J. N. Bahcall, R. Doxsey, D. P. Schneider, N. A. Bahcall, O. Lahav, and B. Yanny, "Gravitational lensing of quasars as seen by the Hubble space telescope snapshot survey," 1992.

[16] C. W. Misner, "The Isotropy of the universe," *Astrophys. J.*, vol. 151, pp. 431–457, 1968.

[17] F. Zwicky, "Nebulae as gravitational lenses," *Phys. Rev.*, vol. 51, p. 290, 1937.

[18] V. C. Rubin and W. K. Ford, Jr., "Rotation of the Andromeda Nebula from a Spectroscopic Survey of Emission Regions," *Astrophys. J.*, vol. 159, pp. 379–403, 1970.

[19] V. C. Rubin, N. Thonnard, and W. K. Ford, Jr., "Rotational properties of 21 SC galaxies with a large range of luminosities and radii, from NGC 4605 /R = 4kpc/ to UGC 2885 /R = 122 kpc/," *Astrophys. J.*, vol. 238, p. 471, 1980.

[20] M. Milgrom, "Dynamics with a non-standard inertia-acceleration relation: an alternative to dark matter," *Annals Phys.*, vol. 229, pp. 384–415, 1994.

[21] P. Hut, "Limits on Masses and Number of Neutral Weakly Interacting Particles," *Phys. Lett.*, vol. B69, p. 85, 1977.

[22] B. W. Lee and S. Weinberg, "Cosmological Lower Bound on Heavy Neutrino Masses," *Phys. Rev. Lett.*, vol. 39, pp. 165–168, 1977.

[23] R. Holman, G. Lazarides, and Q. Shafi, "Axions and the Dark Matter of the Universe," *Phys. Rev.*, vol. D27, p. 995, 1983.

[24] J. Preskill, M. B. Wise, and F. Wilczek, "Cosmology of the Invisible Axion," *Phys. Lett.*, vol. B120, pp. 127–132, 1983.

[25] D. J. Eisenstein *et al.*, "Detection of the baryon acoustic peak in the large-scale correlation function of SDSS luminous red galaxies," *Astrophys.J.*, vol. 633, pp. 560–574, 2005.

[26] J. Dunkley, D. Spergel, E. Komatsu, G. Hinshaw, D. Larson, *et al.*, "Five-Year Wilkinson Microwave Anisotropy Probe (WMAP) Observations: Bayesian Estimation of CMB Polarization Maps," *Astrophys.J.*, vol. 701, p. 1804, 2009.

[27] B. Leibundgut, "Time dilation in the light curve of the distant type ia supernovae sn 1995k," *Astrophys.J.*, vol. 466, p. L21, 1996.

[28] B. Ratra and P. J. E. Peebles, "Cosmological Consequences of a Rolling Homogeneous Scalar Field," *Phys. Rev.*, vol. D37, p. 3406, 1988.

[29] R. R. Caldwell, R. Dave, and P. J. Steinhardt, "Quintessential cosmology: Novel models of cosmological structure formation," *Astrophys. Space Sci.*, vol. 261, pp. 303–310, 1998.

[30] A. A. Starobinsky, "A New Type of Isotropic Cosmological Models Without Singularity," *Phys. Lett.*, vol. B91, pp. 99–102, 1980.

[31] A. H. Guth and E. J. Weinberg, "Cosmological Consequences of a First Order Phase Transition in the SU(5) Grand Unified Model," *Phys. Rev.*, vol. D23, p. 876, 1981.

[32] A. Albrecht and P. J. Steinhardt, "Cosmology for Grand Unified Theories with Radiatively Induced Symmetry Breaking," *Phys. Rev. Lett.*, vol. 48, pp. 1220–1223, 1982.

[33] A. D. Linde, "A New Inflationary Universe Scenario: A Possible Solution of the Horizon, Flatness, Homogeneity, Isotropy and Primordial Monopole Problems," *Phys. Lett.*, vol. B108, pp. 389–393, 1982.

[34] P. J. Steinhardt and N. Turok, "Cosmic evolution in a cyclic universe," *Phys. Rev.*, vol. D65, p. 126003, 2002.

[35] J. Khoury, B. A. Ovrut, P. J. Steinhardt, and N. Turok, "The Ekpyrotic universe: Colliding branes and the origin of the hot big bang," *Phys. Rev.*, vol. D64, p. 123522, 2001.

[36] J. Khoury, P. J. Steinhardt, and N. Turok, "Designing cyclic universe models," *Phys. Rev. Lett.*, vol. 92, p. 031302, 2004.

[37] N. Turok and P. J. Seinhardt, "Beyond inflation: A Cyclic universe scenario," *Phys.Scripta*, vol. T117, pp. 76–85, 2005.

[38] A. Ashtekar, T. Pawlowski, and P. Singh, "Quantum Nature of the Big Bang: Improved dynamics," *Phys. Rev.*, vol. D74, p. 084003, 2006.

[39] Y. Wang and P. Mukherjee, "Observational Constraints on Dark Energy and Cosmic Curvature," *Phys. Rev.*, vol. D76, p. 103533, 2007.

[40] S. Kumar and L. Xu, "Observational constraints on variable equation of state parameters of dark matter and dark energy after Planck," *Phys. Lett.*, vol. B737, pp. 244–247, 2014.

[41] A. A. Penzias and R. W. Wilson, "A Measurement of excess antenna temperature at 4080-Mc/s," *Astrophys. J.*, vol. 142, pp. 419–421, 1965.

[42] P. Mukherjee, A. J. Banday, A. Riazuelo, K. M. Gorski, and B. Ratra, "COBE-DMR-Normalized dark energy cosmogony," *Astrophys. J.*, vol. 598, pp. 767–778, 2003.

[43] S. Perlmutter and B. P. Schmidt, "Measuring cosmology with supernovae," *Lect. Notes Phys.*, vol. 598, pp. 195–217, 2003.

[44] J. L. Tonry *et al.*, "Cosmological results from high-z supernovae," *Astrophys. J.*, vol. 594, pp. 1–24, 2003.

[45] R. C. Tolman, *Relativity, Thermodynamics and Cosmology.* Claredon Press, Oxford, UK, 1934.

[46] R. H. Dicke and P. J. E. Peebles, "The big bang cosmology: Enigmas and nostrums," in *General Relativity: An Einstein Centenary Survey*, 1979.

[47] P. J. Steinhardt and N. Turok, "A Cyclic model of the universe," 2001.

[48] S. Mukherji and M. Peloso, "Bouncing and cyclic universes from brane models," *Phys. Lett.*, vol. B547, pp. 297–305, 2002.

[49] R. Penrose, "Causality, quantum theory and cosmology," *On Space and Time*, pp. 141–195, 2008.

[50] R. Penrose, "The Basic Ideas of Conformal Cyclic Cosmology," *Death and Anti-Death*, vol. 6, pp. 223–242, 2009.

[51] V. G. Gurzadyan and R. Penrose, Sir, "Concentric circles in WMAP data may provide evidence of violent pre-Big-Bang activity," 2010.

[52] R. Penrose, *Cycles of time: An extraordinary new view of the universe.* The Bodley Head, 2010.

[53] V. Sahni and A. Toporensky, "Cosmological Hysteresis and the Cyclic Universe," *Phys.Rev.*, vol. D85, p. 123542, 2012.

[54] V. Sahni, Y. Shtanov, and A. Toporensky, "Arrow of time in dissipationless cosmology," *arXiv-1506.01247*, 2015.

[55] M. Madsen and G. Ellis, "Evolution of the density parameter in inflationary universes," *Monthly Notices of the Royal Astronomical Society*, vol. 234, no. 1, pp. 67–77, 1992.

[56] G. F. R. Ellis and R. Maartens, "The emergent universe: inflationary cosmology with no singularity," *Class. Quant. Grav.*, vol. 21, p. 223, 2004.

[57] G. F. R. Ellis, J. Murugan, and C. G. Tsagas, "The Emergent universe: An Explicit construction," *Class. Quant. Grav.*, vol. 21, pp. 233–250, 2004.

[58] E. I. Guendelman and P. Labrana, "Connecting the nonsingular origin of the universe, the vacuum structure and the cosmological constant problem," in *Proceedings, 13th Marcel Grossmann Meeting on Recent Developments in Theoretical and Experimental General Relativity, Astrophysics, and Relativistic Field Theories (MG13)*, pp. 1608–1610, 2015.

[59] P. A. R. Ade *et al.*, "Planck 2015 results. XX. Constraints on inflation," 2015.

[60] P. J. Steinhardt, "A quintessential introduction to dark energy," *Phil. Trans. Roy. Soc. Lond.*, vol. A361, pp. 2497–2513, 2003.

[61] J. Khoury and A. Weltman, "Chameleon cosmology," *Phys. Rev.*, vol. D69, p. 044026, 2004.

[62] J. Khoury and A. Weltman, "Chameleon fields: Awaiting surprises for tests of gravity in space," *Phys. Rev. Lett.*, vol. 93, p. 171104, 2004.

[63] P. Brax, C. van de Bruck, A.-C. Davis, J. Khoury, and A. Weltman, "Detecting dark energy in orbit - The Cosmological chameleon," *Phys. Rev.*, vol. D70, p. 123518, 2004.

[64] P. Brax, C. van de Bruck, A. C. Davis, J. Khoury, and A. Weltman, "Chameleon dark energy," *AIP Conf. Proc.*, vol. 736, pp. 105–110, 2005. [,105(2004)].

[65] J. D. Barrow and M. P. Dabrowski, "Oscillating Universes," *Mon. Not. Roy. Astron. Soc.*, vol. 275, pp. 850–862, 1995.

[66] M. J. Rees, "The collapse of the universe: an eschatological study," *The Observatory*, vol. 89, pp. 193–198, 1969.

[67] G. F. R. Ellis, J. Hwang, and M. Bruni, "Covariant and Gauge Independent Perfect Fluid Robertson-Walker Perturbations," *Phys. Rev.*, vol. D40, pp. 1819–1826, 1989.

[68] G. F. R. Ellis and M. Bruni, "Covariant and Gauge Invariant Approach to Cosmological Density Fluctuations," *Phys. Rev.*, vol. D40, pp. 1804–1818, 1989.

[69] J. Ehlers, "Contributions to the relativistic mechanics of continuous media," *Gen. Rel. Grav.*, vol. 25, pp. 1225–1266, 1993. [Abh. Akad. Wiss. Lit. Mainz. Nat. Kl.11,793(1961)].

[70] G. F. R. Ellis, "General relativity and cosmology", In *General Relaticity and Cosmology,* Varenna Course No. XLVII. 1971. Reprinted as Golden Oldie, *General Relativity and Gravitation* **41**:581-660 (2009).

[71] A. D. Linde, "Eternal Chaotic Inflation," *Mod. Phys. Lett.*, vol. A1, p. 81, 1986.

[72] A. D. Linde, "Chaotic Inflation," *Phys. Lett.*, vol. B129, pp. 177–181, 1983.

[73] R. H. Brandenberger and J. H. Kung, "Chaotic Inflation as an Attractor in Initial Condition Space," *Phys. Rev.*, vol. D42, pp. 1008–1015, 1990.

[74] M. Takada and O. Dore, "Geometrical Constraint on Curvature with BAO experiments," 2015.

[75] P. Bull, S. Camera, A. Raccanelli, C. Blake, P. Ferreira, M. Santos, and D. J. Schwarz, "Measuring baryon acoustic oscillations with future SKA surveys," *PoS*, vol. AASKA14, p. 024, 2015.

[76] t. U. o. T. University of British Columbia, McGill University and the Dominion Radio Astrophysical Observatory, "The Canadan Hydrogen Intensity Mapping Experiment," 2015.

[77] J. Sievers, "HIRAX: The Hydrogen Intensity and Real-Time Analysis eXperiment," 2015.

[78] G. F. R. Ellis and M. S. Madsen, "Exact scalar field cosmologies," *Class. Quant. Grav.*, vol. 8, p. 667, 1991.

[79] K. Array *et al.*, "BICEP2 / Keck Array VI: Improved Constraints On Cosmology and Foregrounds When Adding 95 GHz Data From Keck Array," 2015.

[80] R. Easther, J. Frazer, H. V. Peiris, and L. C. Price, "Simple predictions from multifield inflationary models," *Phys. Rev. Lett.*, vol. 112, p. 161302, 2014.

[81] L. C. Price, H. V. Peiris, J. Frazer, and R. Easther, "Designing and testing inflationary models with Bayesian networks," 2015.

[82] A. Borde, A. H. Guth, and A. Vilenkin, "Inflationary space-times are incompletein past directions," *Phys. Rev. Lett.*, vol. 90, p. 151301, 2003.

[83] A. Ashtekar and P. Singh, "Loop Quantum Cosmology: A Status Report," *Class. Quant. Grav.*, vol. 28, p. 213001, 2011.

[84] J. D. Barrow and D. Sloan, "Bouncing Anisotropic Universes with Varying Constants," *Phys. Rev.*, vol. D88, no. 2, p. 023518, 2013.

[85] J. T. Nielsen, A. Guffanti, and S. Sarkar, "Marginal evidence for cosmic acceleration from Type Ia supernovae," 2015.

[86] J. H. Steffen, "Constraints on chameleons and axion-like particles from the GammeV experiment," *PoS*, vol. IDM2008, p. 064, 2008.

[87] J. H. Steffen, "The CHASE laboratory search for chameleon dark energy," *PoS*, vol. ICHEP2010, p. 446, 2010.

[88] P. Brax, "Testing Chameleon Fields with Ultra Cold Neutron Bound States and Neutron Interferometry," *Phys. Procedia*, vol. 51, pp. 73–77, 2014.

[89] T. P. Waterhouse, "An Introduction to Chameleon Gravity," 2006.

A Chaotic Cyclic Universe

A.1 Einstein to Friedmann and Raychaudhuri

Starting with the Einstein Field equations written in the compact form;

$$G_{\mu\nu} = R_{\mu\nu} - \frac{1}{2}g_{\mu\nu}R. \tag{A.1a}$$

Here $R = g_{\mu\nu}R_{\mu\nu}$ is the scalar curvature, $R_{\mu\nu}$ is the Ricci tensor and $g_{\mu\nu}$ is the metric tensor. This can also be written in the mixed form, as follows;

$$G^{\mu}_{\nu} = R^{\mu}_{\nu} - \frac{1}{2}\delta^{\mu}_{\nu}R. \tag{A.1b}$$

Note that $g^{\mu\lambda}g_{\lambda\nu} = g^{\mu}_{\nu} = \delta^{\mu}_{\nu}$, giving Kronecker delta. Now use the covariant energy-momentum tensor T^{μ}_{ν} to represent the source term, and surmise that it can be coupled to the field equations as

$$G^{\mu}_{\nu} = 8\pi G T^{\mu}_{\nu}, \tag{A.2}$$

with G Newton's gravitational constant. Substituting this into equation A.1b, one obtains

$$R^{\mu}_{\nu} - \frac{1}{2}\delta^{\mu}_{\nu}R = 8\pi G T^{\mu}_{\nu}. \tag{A.3}$$

Contracting the indices then gives R = -8π GT. Substituting this into equation A.3 finally gives

$$R^{\mu}_{\nu} = 8\pi G(T^{\mu}_{\nu} - \frac{1}{2}\delta^{\mu}_{\nu}T). \tag{A.4}$$

It can be seen that by calculating the explicit terms of the Ricci tensor

$$R^{0}_{0} = -3\frac{\ddot{a}}{a}, \tag{A.5a}$$

and

$$R^{1}_{1} = -\frac{2\dot{a}^2 + S\ddot{a} + 2k}{a^2}, \tag{A.5b}$$

where a is the Roberston-Walker scale factor. Using these terms and the fact that the energy-momentum tensor $T^{\mu}_{\nu} = diag(\rho, -p, -p, -p)$, one finds that equation A.4 becomes

$$-3\frac{\ddot{a}}{a} = 8\pi G\frac{1}{2}(\rho + 3p), \qquad \text{for } \mu = \nu = 0; \tag{A.6a}$$

$$-\frac{2\dot{a}^2 + a\ddot{a} + 2k}{a^2} = 8\pi G\frac{1}{2}(p - \rho), \qquad \text{for } \mu = \nu = 1; \tag{A.6b}$$

where ρ is the total energy density and p is the total pressure. Rearranging these, one arrives at the Friedmann and Raychaudhuri equations, respectively;

$$3H^2 = x\rho - 3K; \tag{A.7}$$

$$3\dot{H} + 3H^2 + \frac{x}{2}(\rho + 3p) = 0. \tag{A.8}$$

Using these two equations, one can now find the conservation equation for matter in an expanding universe. First rewrite equation 2.4 as

$$\dot{a}^2 = \frac{x}{3}a^2\rho - k, \tag{A.9a}$$

and find the derivative with respect to time.

$$2\dot{a}\ddot{a} = \frac{x}{3}(\dot{\rho}a^2 + 2a\dot{a}\rho) \tag{A.9b}$$

Then use equation A.6a to eliminate $\ddot{a}$ to find the conservation equation;

$$\dot{\rho} + 3H(\rho + p) = 0 \tag{A.10}$$

It is interesting to note that given any two of these three equations, the third can be derived, that is to say they are dependant on each other.

B Kicking Chameleons

B.1 Derivation of the equation of motion

In Chameleon gravity, one has that the space-time metric ${g^*}_{\mu\nu}$ is conformally related to the Einstein metric $\tilde{g}_{\mu\nu}$;

$$\tilde{g}_{\mu\nu} = e^{2\beta\phi/M_{pl}} g^*_{\mu\nu} \tag{B.1}$$

Here β is a dimensionless coupling constant ϕ is the Chameleon field and $M_{pl} = (8\pi G)^{-1/2}$. The action is written as

$$S = \int d^4x\sqrt{-g_*}\Big[\frac{M_{pl}^2}{2} - \frac{1}{2}(\nabla_*\phi)^2 - V(\phi)\Big] + \int d^4x\mathcal{L}_m(\tilde{\psi}_m, \tilde{g}_{\mu\nu}). \tag{B.2}$$

Note that

$$S_m = \int d^4x\mathcal{L}_m(\tilde{\psi}_m, \tilde{g}_{\mu\nu}) \tag{B.3}$$

Dropping the * for convenience, one then obtains

$$S = \int d^4x\sqrt{-g}\Big[\frac{M_{pl}^2}{2} - \frac{1}{2}(\partial\phi)^2 - V(\phi) + \frac{1}{\sqrt{-g}}\mathcal{L}_m(\tilde{\psi}_m, \tilde{g}_{\mu\nu}). \tag{B.4}$$

One now wishes to vary this action with respect to ϕ;

$$\partial S = \int d^4x\sqrt{-g}\Big[- \nabla_\mu\phi\delta\nabla^\mu\phi - V_{,\phi}\delta\phi - \frac{1}{\sqrt{-g}}\frac{d\mathcal{L}_m}{d\phi}\partial\phi\Big]; \tag{B.5}$$

$$= \int d^4x\sqrt{-g}\Big[- \nabla_\mu\phi\nabla^\mu\delta\phi - V_{,\phi}\delta\phi - \sum_i \frac{1}{\sqrt{-g}}\frac{\partial\mathcal{L}_m}{\partial\tilde{g}_{\mu\nu}}\frac{\partial\tilde{g}_{\mu\nu}}{\partial\phi}\delta\phi\Big]; \tag{B.6}$$

$$= \int d^4x\sqrt{-g}\Big[(\nabla_\mu\nabla^\mu)\delta\phi - V_{,\phi}\delta\phi - \sum_i \frac{1}{\sqrt{-g}}\frac{\partial\mathcal{L}_m}{\partial\tilde{g}_{\mu\nu}}\frac{2\beta\phi}{M_{pl}}\partial\tilde{g}_{\mu\nu}\delta\phi\Big]; \tag{B.7}$$

$$= \int d^4x\sqrt{-g}\Big[\nabla^2\phi - V_{,\phi}\delta\phi - \sum_i \frac{1}{\sqrt{-g}}\frac{\partial\mathcal{L}_m}{\partial\tilde{g}_{\mu\nu}}\frac{2\beta\phi}{M_{pl}}\tilde{g}_{\mu\nu}\delta\phi\Big]. \tag{B.8}$$

In line 3, the following calculation was used;

$$\int d^4x\nabla_\mu\phi\nabla^\mu\delta\phi = \nabla_\mu\delta\phi| - \int d^4x(\nabla_\mu\nabla^\mu)\delta\phi, \tag{B.9}$$

with $\nabla_\mu\phi \to 0$ and $\delta\phi \to 0$ at the spacetime bounds.

Setting $\delta S = 0$, one obtains;

$$\nabla^2\phi = V_{,\phi}\delta\phi + \sum_i \frac{1}{\sqrt{-g}}\frac{\partial\mathcal{L}_m}{\partial\tilde{g}_{\mu\nu}}\frac{2\beta\phi}{M_{pl}}\tilde{g}_{\mu\nu}. \tag{B.10}$$

Define

$$T_{\mu\nu} \equiv \frac{-2}{\sqrt{-g}}\frac{\delta S_m}{\delta g^{\mu\nu}}. \tag{B.11}$$

It follows that in the Jordan frame one has

$$\tilde{T}_{\mu\nu} \equiv \frac{-2}{\sqrt{-\tilde{g}}}\frac{\delta S_m}{\delta \tilde{g}^{\mu\nu}}. \tag{B.12}$$

The conformal relationship implies

$$T^{\mu}_{\nu} \equiv e^{4\beta\phi/M_{pl}}\tilde{T}^{\mu}_{\nu}. \tag{B.13}$$

Similarly

$$\rho \equiv e^{4\beta\phi/M_{pl}}\tilde{\rho}. \tag{B.14}$$

The equation of state parameter is therefore the same in both frames, $w \equiv p/\rho$.
Assuming matter fields don't interact,

$$\tilde{\nabla}_\nu T^{\mu\nu} = 0. \tag{B.15}$$

With matter a perfect isentropic (work transferred in system frictionless and so entropy constant) field, $\tilde{p} = w_i\tilde{\rho}$. One therefore has

$$\tilde{T}^{\mu\nu}\tilde{g}_{\mu\nu} = -\tilde{\rho} + 3\tilde{p} = -(1 - 3w_i)\tilde{p}. \tag{B.16}$$

Next one imposes a FLRW background metric, with $\rho \propto a^{-3(1+w_i)}$.

$$\begin{aligned}
\tilde{a} &\equiv e^{\beta_i\phi/M_{pl}}a \\
\tilde{g}_{\mu\nu} &= e^{2\beta_i\phi/M_{pl}}g_{\mu\nu} = e^{2\beta_i\phi/M_{pl}}diag(-1, a^2, a^2, a^2) \\
&= diag(-e^{2\beta_i\phi/M_{pl}}, \tilde{a}^2, \tilde{a}^2, \tilde{a}^2) \\
\tilde{g}^{\mu\nu} &= diag(-e^{2\beta_i\phi/M_{pl}}, -\tilde{a}^2, -\tilde{a}^2, -\tilde{a}^2)
\end{aligned} \tag{B.17}$$

Computing the Christoffel symbols;

$$\begin{aligned}
\tilde{\Gamma}^i_{0i} &= \frac{1}{2}\tilde{g}^{1\alpha}(\tilde{g}_{\alpha 0,1} + \tilde{g}_{\alpha 1,0} - \tilde{g}_{01,\alpha} \\
&= \frac{1}{2}\tilde{a}^2(0 + \frac{d}{dt}\tilde{a}^2 + 0) \\
&= \tilde{a}^{-1}\tilde{a}_{,0}
\end{aligned} \tag{B.18}$$

$$\begin{aligned}
\tilde{\Gamma}^0_{ii} &= \frac{1}{2}\tilde{g}^{0\alpha}(2\tilde{g}_{\alpha 1,1} - \tilde{g}_{11,\alpha}) \\
&= -\frac{1}{2}e^{2\beta_i\phi/M_{pl}}(-2\tilde{a}\tilde{a}_{,0}) \\
&= e^{2\beta_i\phi/M_{pl}}\tilde{a}\tilde{a}_{,0}.
\end{aligned} \tag{B.19}$$

Next expand the conservation equation, $B.15$;

$$
\begin{aligned}
0 = \tilde{\nabla}_\nu \tilde{T}^{0\nu} &= \tilde{T}^{0\nu}_{,\nu} + \tilde{\Gamma}^0_{\sigma\nu}\tilde{T}^{\sigma\nu} + \tilde{\Gamma}^\nu_{\sigma\nu}\tilde{T}^{0\sigma} \\
&= \tilde{T}^{00}_{,0} + \tilde{\Gamma}^0_{\sigma\nu}\tilde{T}^{\sigma\nu} + \tilde{\Gamma}^\nu_{0\nu}\tilde{T}^{00} \\
&= (-\tilde{\rho}\tilde{g}^{00})_{,0} + 3e^{-2\beta_i\phi/M_{pl}}\tilde{a}\tilde{a}_{,0}\tilde{p}\tilde{g}^{11} + 3\tilde{a}^{-1}\tilde{a}_{,0}(-\tilde{\rho}\tilde{g}^{00}) \\
&= e^{-2\beta_i\phi/M_{pl}}(\tilde{\rho}_{,0} + 3\tilde{a}^{-1}\tilde{a}_{,0}\tilde{p} + 3\tilde{a}^{-1}\tilde{a}_{,0}\tilde{\rho}) \\
&= e^{-2\beta_i\phi/M_{pl}}(\tilde{\rho}_{,0} + 3(1+w_i)\tilde{a}^{-1}\tilde{a}_{,0}\tilde{\rho})
\end{aligned}
\tag{B.20}
$$

Multiplying through by $e^{2\beta_i\phi/M_{pl}}\tilde{a}^{3(1+w_i)}$;

$$
\begin{aligned}
0 &= \tilde{a}^{3(1+w_i)}\tilde{\rho}_{,0} + 3(1+w_i)\tilde{a}^{3(1+w_i)^{-1}}\tilde{a}_{,0}\tilde{\rho} \\
&= (\tilde{a}^{3(1+w_i)}\tilde{\rho})_{,0} \\
&= (a^{3(1+w_i)}e^{3(1+w_i)\beta_i\phi/M_{pl}})_{,0}.
\end{aligned}
\tag{B.21}
$$

Therefore,

$$
\rho \equiv e^{3(1+w_i)\beta_i\phi/M_{pl}}\tilde{\rho}. \tag{B.22}
$$

The energy density for different matter species i in the Einstein frame is therefore

$$
\begin{aligned}
\rho_i &= -e^{3(1+w_i)\beta_i\phi/M_{pl}}\frac{1}{1-3w_i}T^{\mu\nu}_{(i)}g^{(i)}_{\mu\nu} \\
&= e^{3(1+w_i)\beta_i\phi/M_{pl}}\frac{1}{1-3w_i}\frac{2}{\sqrt{-g^{(i)}}}\frac{\partial\mathcal{L}_m}{\partial g^{(i)}_{\mu\nu}}g^{(i)}_{\mu\nu} \\
&= e^{3(1+w_i)\beta_i\phi/M_{pl}}\frac{1}{1-3w_i}\frac{2}{\sqrt{e^{8\beta_i\phi/M_{pl}}(-g)}}\frac{\partial\mathcal{L}_m}{\partial g^{(i)}_{\mu\nu}}g^{(i)}_{\mu\nu} \\
&= e^{3(1+w_i)\beta_i\phi/M_{pl}}\frac{1}{1-3w_i}\frac{2}{\sqrt{-g}}\frac{\partial\mathcal{L}_m}{\partial g^{(i)}_{\mu\nu}}.
\end{aligned}
\tag{B.23}
$$

Substituting the above into equation $B.10$, one obtains

$$
\nabla^2\phi = V_{,\phi} + \sum_i (1-3w_i)\frac{\beta_i}{M_{pl}}\rho_i e^{(1-3w_i)\beta_i\phi/M_{pl}}. \tag{B.24}
$$

Next one defines the effective potential;

$$
V_{eff}(\phi) = V(\phi) + \sum_i \rho_i e^{(1-3w_i)\beta_i\phi/M_{pl}} \tag{B.25}
$$

It follows that

$$
\nabla^2 = V_{eff,\phi}(\phi). \tag{B.26}
$$

One expects ϕ to seek a minimum for $V_{eft}(\phi)$. One also wishes to have a $V(\phi)$ that gives rise to cosmic acceleration via the slow roll mechanism. One assumes it has been rolling down the slope in the positive direction, and so ϕ is a monotonically decreasing function.

For Chameleon behaviour, one requires;

1. $\lim_{\phi\to 0} V(\phi) = \infty$;
2. $V(\phi)$ is C^∞, bounded below and strictly decreasing;
3. $V_{,\phi}(\phi)$ is strictly negative and increasing;

4. $V_{,\phi\phi}(\phi)$ is strictly positive and decreasing.

In FLRW;

$$\begin{aligned}\nabla^2\phi &= g^{\mu\nu}\nabla_m u\nabla_\nu\phi \\ &= g^{\mu\nu}\partial_\mu\partial_\nu - g^{\mu\nu}\Gamma^\rho_{\nu\mu}\phi_{,\rho} \\ &= g^{00}\partial_0\partial_0\phi - (g^{11}\Gamma^0_{11} + g^{22}\Gamma^0_{22} + g^{33}\Gamma^0_{33})\phi_{,0} \\ &= -\ddot{\phi} - a^{-2}3a\dot{a}\dot{\phi} \\ &= -(\ddot{\phi} + 3H\dot{\phi}).\end{aligned} \tag{B.27}$$

One therefore obtains the equation of motion for ϕ;

$$\ddot{\phi} + 3H\dot{\phi} = -V_{eff,\phi}(\phi) \tag{B.28}$$

This requires further manipulation in order to obtain the desired equation;

$$\begin{aligned}\ddot{\phi} + 3H\dot{\phi} = -V_{,\phi} - \sum_i \rho_i(1-3w_i)\frac{\beta_1}{M_{pl}}e^{(1-3w_i)\beta_i\phi/M_{pl}} \\ = -V_{,\phi} - \sum_i T^\mu_{(i)\nu}\frac{\beta_1}{M_{pl}}e^{(1-3w_i)\beta_i\phi/M_{pl}}\end{aligned} \tag{B.29}$$

Consider matter and radiation, $i = m$ and r with $\beta_i = \beta$.

$$\ddot{\phi} + 3H\dot{\phi} = -V_{,\phi} - \frac{\beta}{M_{pl}}\big[\rho_r(1-3w_r)e^{(1-3w_r)\beta\phi/M_{pl}} + \rho_m(1-3w_m)e^{(1-3w_m)\beta\phi/M_{pl}}\big] \tag{B.30}$$

For convenience, define $\Sigma = (1-3w_r) = \frac{1}{\rho_r}(\rho_r - 3p_r)$ and $f_m = \frac{\rho_m}{\rho_r}$.

$$\begin{aligned}\ddot{\phi} + 3H\dot{\phi} &= -V_{,\phi} - \frac{\beta}{M_{pl}}\big[\frac{\rho_r - 3p_r}{\rho_r}e^{(1-3w_r)\beta\phi/M_{pl}} + \frac{\rho_m}{\rho_r}^{\beta\phi/M_{pl}}\big] \\ &= -V_{,\phi} - \frac{\beta}{M_{pl}}\big[\Sigma e^{(1-3w_r)\beta\phi/M_{pl}} + f_m^{\beta\phi/M_{pl}}\big]\end{aligned} \tag{B.31}$$

The Einstein field equations can be written

$$G^{\mu\nu} = \frac{1}{M_{pl}^2}T^{\mu\nu}, \tag{B.32}$$

with

$$T^{\mu\nu} = T^{\mu\nu}_\phi + \sum_i T^{\mu\nu}_{(i)}. \tag{B.33}$$

Here for scalars

$$T^{\mu\nu}_\phi = \partial^\mu\phi\partial^\nu\phi - (\frac{1}{2}\partial_\alpha\phi\partial^\alpha\phi + V)g^{\mu\nu}. \tag{B.34}$$

Consider the 00 case, with $R = \frac{6}{a^2}(\ddot{a}a + \dot{a}^2)$;

$$\begin{aligned}G^{00} &= R^{00} - \frac{1}{2}Rg^{00} \\ &= R^{00} + \frac{3}{a^2}(\ddot{a}a + \dot{a}^2) \\ &= 3H^2.\end{aligned} \tag{B.35}$$

Here the following is used;

$$\begin{aligned} R^{00} &= -\Gamma^{\alpha}_{00,\alpha} + \Gamma^{\alpha}_{0\alpha,0} + \Gamma^{\alpha}_{\sigma 0}\Gamma^{\sigma}_{\alpha 0} - \Gamma^{\alpha}_{\sigma\alpha}\Gamma^{\sigma}_{00} \\ &= \Big(\frac{1}{2}g^{\alpha\sigma}(g_{\sigma 0,\alpha} + g_{\sigma\alpha,0} - g_{\alpha 0,\sigma})\Big) + \sum_i \Gamma^{i}_{j0}\Gamma^{j}_{0i} \\ &= -\sum_i \big(\frac{1}{2}a^{-2}(2a\dot{a})\big)_{,0} + \sum_i (\Gamma^{i}_{i0})^2 \\ &= 3\Big(\frac{\dot{a}}{a}\Big)_{,0} + 3\Big(\frac{\dot{a}}{a}\Big)^2 \\ &= -3\Big(\frac{\ddot{a}}{a} - \Big(\frac{\dot{a}}{a}\Big)^2\Big) + 3\Big(\frac{\dot{a}}{a}\Big)^2 \\ &= -3\frac{\ddot{a}}{a}. \end{aligned} \tag{B.36}$$

Looking again at the stress energy tensor;

$$\begin{aligned} T^{\mu\nu}_{(i)} &\equiv -\frac{2}{\sqrt{g}}\frac{\partial\mathcal{L}}{\partial g_{\mu\nu}} \\ &= -\frac{2}{\sqrt{-\tilde{g}e^{-8\beta_i\phi}}}\frac{\partial\mathcal{L}}{\partial\tilde{g}_{\mu\nu}}\frac{\partial\tilde{g}^{\mu\nu}}{\partial g^{\mu\nu}} \\ &= -\frac{2}{\sqrt{-\tilde{g}}}\frac{\partial\mathcal{L}}{\partial\tilde{g}_{\mu\nu}}e^{6\beta_i\phi/M_{pl}} \\ &= \tilde{T}^{\mu\nu}e^{6\beta_i\phi/M_{pl}}. \end{aligned} \tag{B.37}$$

One then finds the 00-component;

$$T^{00}_{(i)} = \tilde{T}^{00}\tilde{g}^{00}\frac{e^{6\beta_i\phi/M_{pl}}}{\tilde{g}^{00}} = \tilde{\rho}e^{4\beta_i\phi/M_{pl}} = \rho_i e^{(1-3w_i)\beta_i\phi/M_{pl}} \tag{B.38}$$

For radiation and matter, one has

$$T^{00}_{r} = \rho_i e^{(1-3w_r)\beta_i\phi/M_{pl}}; \tag{B.39a}$$

$$T^{00}_{m} = \rho_i e^{(1-3w_m)\beta_i\phi/M_{pl}}. \tag{B.39b}$$

The full expression for T^{00} is therefore,

$$T^{00} = \frac{1}{2}\dot{\phi}^2 + V(\phi) + \rho_r e^{\Sigma\beta_i\phi/M_{pl}} + \rho_m e^{\beta_i\phi/M_{pl}}. \tag{B.40}$$

Note that from the Einstein Equations and from Equation $B.35$,

$$3H^2 = G^{00} = \frac{1}{M_{pl}}^2 T^{00}. \tag{B.41}$$

Finally one obtains the first Friedman equation.

$$3M^2_{pl}H^2 = \frac{1}{2}\dot{\phi}^2 + V(\phi) + \rho_r e^{\Sigma\beta_i\phi/M_{pl}} + \rho_m e^{\beta_i\phi/M_{pl}} \tag{B.42}$$

Next one requires the trace of G;

$$G^{\mu}_{\mu} = G^{\mu\nu}g_{\mu\nu} = R^{\mu\nu}g_{\mu\nu} - \frac{1}{2}g^{\mu\nu}g_{\mu\nu} = R - \frac{1}{2}(4R) = -R = \frac{6}{a^2}(\ddot{a}a + \dot{a}^2). \tag{B.43}$$

One also has

$$\begin{aligned} T^{\mu\nu}g_{\mu\nu} &= \tilde{T}^{\mu\nu}e^{6\beta_i\phi/M_{pl}}\tilde{g}_{\mu\nu}e^{-2\beta_i\phi/M_{pl}} \\ &= -(1-3w_i)\tilde{\rho}e^{4\beta_i\phi/M_{pl}} \\ &= -(1-3w_i)\rho e^{-3(1+w_i)\beta_i\phi/M_{pl}}e^{4\beta_i\phi/M_{pl}} \\ &= (1-3w_i)\rho e^{(1-3w_i)\beta_i\phi/M_{pl}}; \end{aligned} \tag{B.44}$$

$$\begin{aligned} T^{\mu\nu}_{(r)}g_{\mu\nu} &= -\Sigma\rho_r e^{\Sigma\beta_i\phi/M_{pl}}; \\ T^{\mu\nu}_{(m)}g_{\mu\nu} &= -\rho_m e^{\beta_i\phi/M_{pl}}; \end{aligned} \tag{B.45}$$

$$T^{\mu\nu}_{\phi}g_{\mu\nu} = \partial_\nu\phi\partial^\nu\phi - \Big(\frac{1}{2}\partial_\nu\phi\partial^\nu\phi + V\Big)g_{\mu\nu}g^{\mu\nu} = -\partial_\nu\phi\partial^\nu\phi - 4V = \dot{\phi}^2 - 4V. \tag{B.46}$$

One therefore obtains

$$\begin{aligned} G^\mu_\mu &= \frac{1}{M_{pl}}(T^\mu_{(\phi)\mu} + \sum_i T^\mu_{(i)\mu} \\ \Rightarrow -6M^2_{pl}\Big[\frac{\ddot{a}}{a} - \Big(\frac{\dot{a}}{a}\Big)^2\Big] &= \dot{\phi}^2 - 4V - \Sigma\rho_r e^{\Sigma\beta_i\phi/M_{pl}} - \rho_m e^{\beta_i\phi/M_{pl}}. \end{aligned} \tag{B.47}$$

This is divided through by 2 and $(\dot{a}/a)^2H^2$ is eliminated using the first Friedman Equation B.42;

$$\begin{aligned} -3M^2_{pl}\Big[\frac{\ddot{a}}{a} + \frac{1}{3}\frac{1}{M^2_{pl}}\Big(\frac{1}{2}\dot{\phi}^2 + V(\phi) + \rho_r e^{\Sigma\beta_i\phi/M_{pl}} + \rho_m e^{\beta_i\phi/M_{pl}}\Big)\Big] = \\ \frac{1}{2}\dot{\phi}^2 - 2V - \frac{1}{2}\Sigma\rho_r e^{\Sigma\beta_i\phi/M_{pl}} - \frac{1}{2}\rho_m e^{\beta_i\phi/M_{pl}} \end{aligned} \tag{B.48}$$

$$\Rightarrow 3M^2_{pl}\frac{\ddot{a}}{a} = V - \dot{\phi}^2 - (1-\Sigma)\rho_r e^{\Sigma\beta_i\phi/M_{pl}} - \frac{1}{2}\rho_m e^{\beta_i\phi/M_{pl}} \tag{B.49}$$

This gives the second Friedman Equation.

Making some approximations now, one has that since $M_{pl} >> \beta\phi$, $e^{\beta_i\phi/M_{pl}} \approx 1$. Also, since $0 \leq \Sigma \leq 1$, $e^{\Sigma\beta_i\phi/M_{pl}} \approx 1$. The equation of motion and Friedman equations become

$$\ddot{\phi} + 3H\dot{\phi} = -V_{,\phi} - \frac{\beta}{M_{pl}}\rho_r(\Sigma + f_m); \tag{B.50}$$

$$3M^2_{pl}H^2 = \frac{1}{2}\dot{\phi}^2 + V(\phi) + \rho_r + \rho_m; \tag{B.51}$$

$$3M^2_{pl}\Big(\frac{\ddot{a}}{a}\Big) = V(\phi) - \dot{\phi}^2 - \rho_r(1 - \frac{1}{2}\Sigma) - \frac{1}{2}\rho_m. \tag{B.52}$$

Now define a new time variable, $N \equiv \ln(a/a_{,i})$ with a prime denoting differentiation with respect to N. The scalar field is also made dimensionless by defining $\varphi \equiv \phi/M_{pl}$. Next, one needs to find the equation of motion in terms of these new variables.

Note that

$$\frac{dN}{dt} = \frac{d}{dt}(\ln a - \ln \dot{a}) = \frac{\dot{a}}{a} = H; \tag{B.53}$$

$$\frac{d}{d\phi} = \frac{d\varphi}{d\phi}\frac{d}{d\varphi} = \frac{1}{M_{pl}}\frac{d}{d\varphi}. \tag{B.54}$$

Also,

$$\dot{\phi} = \frac{d\phi}{dN}\frac{dN}{dt} = \frac{d}{dN}\big(\varphi M_{pl}\big)\frac{dN}{dt} = M_{pl}\varphi' H; \tag{B.55a}$$

$$\ddot{\phi} = \frac{d}{dN}(\dot{\phi})\frac{dN}{dt} = \frac{d}{dN}(M_{pl}\varphi' H)H = M_{pl}H(H'\varphi' + H\varphi''). \tag{B.55b}$$

Using this in the equation of motion;

$$M_{pl}HH'\varphi' + M_{pl}H^2\varphi'' + 3H^2M_{pl}\varphi' = -\frac{dV/d\varphi}{M_{pl}} - \frac{\beta}{M_{pl}}\rho_r(\Sigma + f_m); \tag{B.56}$$

$$\Rightarrow \varphi'' + \Big(3 + \frac{H'}{H}\Big)\varphi' = -\frac{dV/d\varphi}{H^2M_{pl}^2} - \frac{\beta}{H^2M_{pl}^2}\rho_r(\Sigma + f_m). \tag{B.57}$$

Looking at the first Friedman equation, one has

$$\begin{aligned} 3M_{pl}^2H^2 &= \frac{1}{2}H^2M_{pl}^2\varphi'^2 + V(\phi) + \rho_r(1 + f_m); \\ 1 &= \frac{\varphi^2}{6} + \frac{V}{3M_{pl}^2H^2}(1 + f_m). \\ \Rightarrow \frac{\rho_r}{M_{pl}^2H^2} &= 3\Big(1 - \frac{\varphi'^2}{6} - \frac{V}{3M_{pl}^2H^2}\Big)(1 + f_m)^{-1}. \end{aligned} \tag{B.58}$$

One drops $\mathcal{O}({f_m}^2)$ noting that

$$\frac{1}{1 + f_m} = \frac{1 - f_m}{(1 - f_m)(1 + f_m)} = \frac{1 - f_m}{1 - f_m^2} \approx 1 - f_m, \tag{B.59}$$

to obtain

$$\frac{\rho_r}{M_{pl}^2} \approx 3\Big(1 - \frac{\varphi'^2}{6} - \frac{V}{3M_{pl}^2H^2}\Big)(1 - f_m). \tag{B.60}$$

Putting the above into the equation of motion and again dropping $\mathcal{O}({f_m}^2)$;

$$\begin{aligned} \varphi'' + \Big(\frac{H'}{H} + 3\Big)\varphi' &= -\frac{dV/d\varphi}{H^2M_{pl}^2} - 3\beta\Big(1 - \frac{\varphi'^2}{6} - \frac{V}{3M_{pl}^2H^2}\Big)(1 - f_m)(\Sigma + f_m); \\ \varphi'' + \Big(\frac{H'}{H} + 3\Big)\varphi' &= -\frac{dV/d\varphi}{H^2M_{pl}^2} - 3\beta\Big(1 - \frac{\varphi'^2}{6} - \frac{V}{3M_{pl}^2H^2}\Big)(\Sigma + f_m - \Sigma f_m). \end{aligned} \tag{B.61}$$

Eliminate H' using the second Friedmann equation and noting that $\frac{\ddot{a}}{a} = H'H + H^2$;

$$\begin{aligned} 3M_{pl}^2(H'H + H^2) &= V(\phi) - M_{pl}^2H^2\varphi'^2 - \rho_r(1 - \frac{1}{2}\Sigma) - \frac{1}{2}\rho_m; \\ \frac{H'}{H} + 3 &= \frac{V}{3M_{pl}^2H^2} - \frac{\varphi'^2}{3} + \frac{\rho_r}{3M_{pl}^2H^2}\Big(\frac{\Sigma - f_m}{2} - 1\Big) + 2. \end{aligned} \tag{B.62}$$

Substituting sqation $B.58$ into the above, one obtains;

$$\begin{aligned}
\frac{H'}{H}+3 &= \frac{V}{3M_{pl}^2H^2}-\frac{\varphi'^2}{3}+\Big(\frac{\Sigma-f_m}{2}-1\Big)(1-f_m)\Big(1-\frac{\varphi'^2}{6}-\frac{V}{3M_{pl}^2H^2}\Big)+2\\
&= \frac{V}{3M_{pl}^2H^2}-\frac{\varphi'^2}{3}+\Big(\frac{\Sigma+f_m}{2}-\frac{\Sigma f_m}{2}-1\Big)(1-f_m)\Big(1-\frac{\varphi'^2}{6}-\frac{V}{3M_{pl}^2H^2}\Big)+2\\
&= \frac{V}{3M_{pl}^2H^2}-\frac{\varphi'^2}{3}+\Big(\frac{\Sigma+f_m}{2}-1\Big)\Big(1-\frac{\varphi'^2}{6}-\frac{V}{3M_{pl}^2H^2}\Big)+2\\
&= \frac{V}{3M_{pl}^2H^2}-\frac{\varphi'^2}{3}+\frac{\Sigma+f_m}{2}\Big(1-\frac{\varphi'^2}{6}-\frac{V}{3M_{pl}^2H^2}\Big)+1-\frac{\varphi'^2}{6}+\frac{V}{3M_{pl}^2H^2}\\
&= \frac{2V}{3M_{pl}^2H^2}-\frac{\varphi'^2}{6}+1+\frac{\Sigma+f_m}{2}\Big(1-\frac{\varphi'^2}{6}-\frac{V}{3M_{pl}^2H^2}\Big)\\
&= \Big(1+\frac{\Sigma+f_m}{2}\Big)\Big(1-\frac{\varphi'^2}{6}\Big)+\frac{2V}{3M_{pl}^2H^2}\Big(1-\frac{\Sigma+f_m}{4}\Big).
\end{aligned} \tag{B.63}$$

Putting this back into the equation of motion;

$$\begin{aligned}
\varphi''+\Big[\Big(1+\frac{\Sigma+f_m}{2}\Big)\Big(1-\frac{\varphi'^2}{6}\Big)+\frac{2V}{3M_{pl}^2H^2}\Big(1-\frac{\Sigma+f_m}{4}\Big)\Big]\varphi' =\\
-\frac{dV/d\varphi}{M_{pl}^2H^2}-3\beta\Big(1-\frac{\varphi'}{6}-\frac{V}{M_{pl}H^2}\Big)(\Sigma+f_m-\Sigma f_m).
\end{aligned} \tag{B.64}$$

Looking again at the first Friedman Equation;

$$\begin{aligned}
3H^2M_{pl}^2 &= \frac{1}{2}M_{pl}^2H^2\varphi'^2+V+\rho_r(1+f_m)\\
\Rightarrow 1 &= \frac{\varphi'^2}{6}+\frac{V}{3M_{pl}^2H^2}+\frac{1}{3M_{pl}^2H^2}\rho_r(1+f_m)\\
\Rightarrow \frac{1}{M_{pl}^2H^2} &= \frac{3}{\rho_r(1+f_m)+V}\Big(1-\frac{\varphi/^2}{6}\Big).
\end{aligned} \tag{B.65}$$

In order to further simplify the equation of motion, one notes that $\Sigma{\leq}0.1$ and $f_m \leq 10^{-}6$ prior to BBN. From this, $1{+}f_m \approx 1{+}\Sigma \approx 1$.

$$
\begin{aligned}
\varphi''+\varphi'\Big[&\Big(1+\frac{\Sigma+1+f_m+1-2}{2}\Big)\Big(1-\frac{\varphi'^2}{6}\Big)\\
&+\frac{2V}{\rho_r(1+f_m)+V}\Big(1-\frac{\varphi'^2}{6}\Big)\Big(1-\frac{\Sigma+1+f_m+1-2}{4}\Big)\Big]\\
&=-3\frac{3dV/d\varphi}{\rho_r(1+f_m)+V}\Big(1-\frac{\varphi'^2}{6}\Big)\\
&\quad-3\beta\Big[1-\frac{\varphi'^2}{6}-\frac{V}{\rho_r(1+f_m)+V}\Big(1-\frac{\varphi'^2}{6}\Big)\Big)\Big](\Sigma+f_m-\Sigma f_m)\\
&=-3\frac{3dV/d\varphi}{\rho_r(1+f_m)+V}\Big(1-\frac{\varphi'^2}{6}\Big)\\
&\quad-3\beta\Big(1-\frac{\varphi'^2}{6}\Big)\Big(1-\frac{V}{\rho_r+V}\Big)(\Sigma+f_m-\Sigma f_m)\\
\Rightarrow\ \varphi''+\varphi'&\Big(1-\frac{\varphi'^2}{6}\Big)\Big(1+\frac{2V}{\rho_r+V}\Big)\\
&=\Big(1-\frac{\varphi'^2}{6}\Big)\Big[-3\frac{3dV/d\varphi}{\rho_r+V}-3\beta\Big(1-\frac{V}{\rho_r+V}\Big)(\Sigma+f_m)\Big]
\end{aligned}
\tag{B.66}
$$

This result also matches that of Burrage et al.

Burrage et al. then simplify this equation further by excluding the bare potential. They therefore obtain

$$
\frac{\phi''}{1-(\phi')^2/6}+\phi'=-3\beta\Sigma. \tag{B.67}
$$

B.2 Perturbing the Chameleon

Here one adds a perturbation to illustrate the stability of the surfing solution.

B.2.1 Deriving equation of motion

The Einstein frame action, with a perturbation correction, is

$$
S=\int d^4x\sqrt{-g}\left[\frac{M_{Pl}}{2}R+P(X)-V(\phi)-\frac{1}{\sqrt{-g}}\mathcal{L}_m\right], \tag{B.68}
$$

where $X=-\frac{1}{2}(\nabla\phi)^2$. Varying this action, and assuming a RW geometry, leads to the modified Friedman and Klein-Gordon equations;

$$
3M_{Pl}^2H^2=\rho_\phi+\rho_r; \tag{B.69}
$$

$$
M_{Pl}^2\left(H^2+2\frac{\dot a}{a}\right)=-p_\phi-w\rho_r; \tag{B.70}
$$

$$
\partial_t\left(P_{,X}\dot\phi\right)+3HP_{,X}\dot\phi=-V_{,\phi}-\frac{\beta}{M_{Pl}}\Sigma\rho_r; \tag{B.71}
$$

where $\rho_r=\mathrm{e}^{4\beta\phi/M_{Pl}}\tilde\rho_r$ is the Einstein frame energy density of relativistic particles and

$$
\rho_\phi=P_{,X}\dot\phi^2-P+V(\phi); \tag{B.72}
$$

$$
p_\phi=P-V(\phi). \tag{B.73}
$$

Here $P = P(X)$. Choose a perturbation of the form

$$P = X + \alpha X^2 \tag{B.74}$$

$$= \frac{1}{2}\dot{\phi}^2 + \frac{\alpha}{4}\dot{\phi}^4. \tag{B.75}$$

From B.75 it follows that

$$P_{,X} = 1 + 2\alpha X \tag{B.76}$$

$$= 1 + \alpha\dot{\phi}^2 \tag{B.77}$$

and

$$P_{,XX} = 2\alpha. \tag{B.78}$$

Change the time variable to Einstein frame e-folds, and normalise the field, such that

$$\dot{\phi} = M_{Pl} H \varphi' \tag{B.79}$$

and

$$\ddot{\phi} = M_{Pl} H H' \varphi' + M_{Pl} H^2 \varphi''. \tag{B.80}$$

Using B.79 with B.75 B.77 allows one to write B.72 B.73 as

$$\rho_\phi = \frac{1}{2} M_{Pl}^2 H^2 \varphi'^2 + \frac{3\alpha}{4} M_{Pl}^4 H^4 \varphi'^4 + V(\phi); \tag{B.81}$$

$$p_\phi = \frac{1}{2} M_{Pl}^2 H^2 \varphi'^2 + \frac{\alpha}{4} M_{Pl}^4 H^4 \varphi'^4 - V(\phi). \tag{B.82}$$

The terms in B.71 can then be written as

$$\partial_t \left(P_{,X} \dot{\phi} \right) = \dot{P_{,X}} \dot{\phi} + P_{,X} \ddot{\phi} \tag{B.83}$$

$$= P_{,XX} \dot{\phi}^2 \ddot{\phi} + P_{,X} \ddot{\phi} \tag{B.84}$$

$$= \ddot{\phi} \left(1 + 3\alpha \dot{\phi}^2 \right) \tag{B.85}$$

$$= \left(M_{Pl} H H' \varphi' + M_{Pl} H^2 \varphi'' \right) \left(1 + 3\alpha M_{Pl}^2 H^2 \varphi'^2 \right); \tag{B.86}$$

and

$$3 H P_{,X} \dot{\phi} = 3H \left(1 + \alpha \dot{\phi} \right) \tag{B.87}$$

$$= 3 M_{Pl} H^2 \varphi' + 3\alpha M_{Pl}^3 H^4 \varphi'^3; \tag{B.88}$$

and

$$V_{,\phi} = \frac{1}{M_{Pl}} V_{,\varphi}. \tag{B.89}$$

Plugging B.86 B.88 B.89 into B.71, dividing by $M_{Pl} H^2$, and rearranging gives

$$\varphi'' + \varphi' \left[\left(1 + 3\alpha M_{Pl}^2 H^2 \varphi'^2 \right) \left(\frac{H'}{H} + 1 \right) + 3\alpha M_{Pl}^2 H^2 \varphi' \varphi'' + 2 \right] = \frac{-1}{M_{Pl}^2 H^2} \left(V_{,\varphi} + \beta \Sigma \rho_r \right). \tag{B.90}$$

The H'/H term can be eliminated from B.90 by rearranging B.70, which gives

$$\left(\frac{H'}{H}+1\right)=\frac{-p_\phi-w\rho_r}{2M_{Pl}^2H^2}-\frac{1}{2}. \tag{B.91}$$

One requires an expression for $M_{Pl}^2H^2$. From B.69,

$$\left(\varphi'^4\frac{3\alpha}{4}\right)Z^2+\left(\frac{1}{2}\varphi'^2-3\right)Z+\left(\rho_r+V\right)=0, \tag{B.92}$$

where $Z{=}{M_{Pl}}^2H^2$.

For $(\varphi',\alpha)\neq 0$,

$$Z_\pm=\frac{\left(3-\frac{\varphi'^2}{2}\right)\pm\sqrt{\left(3-\frac{\varphi'^2}{2}\right)^2-3\alpha\varphi'^4(\rho_r+V)}}{\frac{3}{2}\alpha\varphi'^4}. \tag{B.93}$$

For real roots one requires

$$\left(3-\frac{\varphi'^2}{2}\right)^2>3\alpha\varphi'^4(\rho_r+V); \tag{B.94}$$

$$\Rightarrow\alpha<\frac{\left(\frac{3}{\varphi'^2}-\frac{1}{2}\right)^2}{3(\rho_r+V)}. \tag{B.95}$$

This seems to limit the allowable limits of α, since $\left|\varphi'^2\right|\leq 6$, giving;

$$\varphi'=0 \text{ corresponds to } \alpha<\infty; \tag{B.96}$$

$$\varphi'=\sqrt{6} \text{ corresponds to } \alpha=0. \tag{B.97}$$

From B.92 one also has that for $\alpha{=}0$;

$$M_{Pl}^2H^2=\frac{\rho_r+V}{3-\frac{\varphi'^2}{2}}. \tag{B.98}$$

Since both possible roots of B.93 are positive, one requires that in the limit that α goes to zero one recovers the above solution. Therefore taking the negative solution, one arrives at the final expression for ${M_{Pl}}^2H^2$;

$$M_{Pl}^2H^2=\frac{\left(3-\frac{\varphi'^2}{2}\right)-\sqrt{\left(3-\frac{\varphi'^2}{2}\right)^2-3\alpha\varphi'^4(\rho_r+V)}}{\frac{3}{2}\alpha\varphi'^4} \qquad \text{for } \varphi'\neq 0 \tag{B.99}$$

$$=\frac{\rho_r+V}{3} \qquad \text{for } \varphi'=0. \tag{B.100}$$

One can numerically solve the scalar EOM B.90 for the field with various initial conditions, and investigate the effect of the perturbation term by changing the value of the parameter α. All results are for an exponential potential of the form

$$V(\phi)=M^4\exp\left[\left(\frac{M}{\phi}\right)^n\right], \tag{B.101}$$

where $M\approx 10^{-3}$eV is fixed by observations. For simplicity, initially assume the kick function Σ is a constant, given by

$$\Sigma=\frac{1}{3\beta^2},; \tag{B.102}$$

and the Einstein frame energy density is

$$\rho_r = \rho_{r,i} \mathrm{e}^{-4N}, \tag{B.103}$$

where $\rho_{r,i}$ is some initial value, at $N = 0$. This is not strictly correct. The full expression for the energy density,

$$\rho_r = \frac{\pi}{30} g_*(T_J) \left[\frac{g_{*S}(T_{J,i})}{g_{*S}(T_J)} \right]^{4/3} T_{J,i}^4 \mathrm{e}^{4(\beta\varphi_i - N)}, \tag{B.104}$$

requires one to evaluate $g_{*S}(T_J)$ which involves integrating over all the distribution functions for the relativistic particles, and summing them. This is not necessary for illustrative purpose though.

B.2.2 Simulation

Upon simulating the perturbed case, one finds (Figure 15) that the results do not differ from that of the normal case, showing that the surfer is stable to small perturbations.

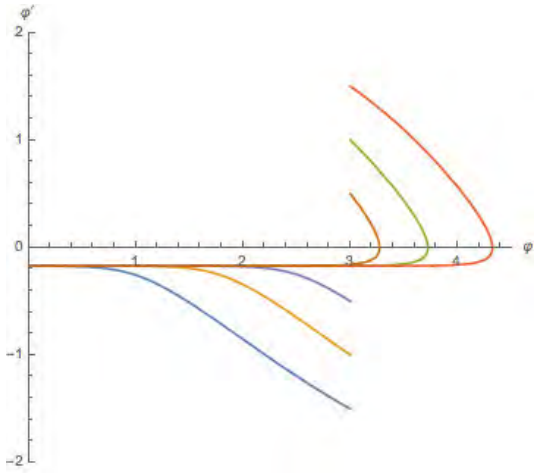

Figure 15: Phase Plane for the Perturbed Chameleon